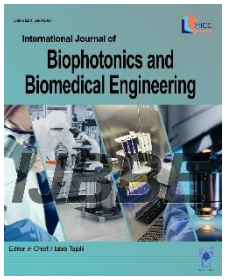

Volume 5, Issue 2, (2025) Article 9

International Journal of

Biophotonicsand Biomedical Engineering (IJBBE)

https://doi.org/10.57647/ijbbe.2025.0502.09

Development of Deep Convolutional Neural Network Algorithms Based on Dense Net Model for Adaptive Classification of Chest Diseases

Vincent Andrew Akpan [1,*], Naheemat Olayemi Raji [2]

[1] *Department of Biomedical Engineering, The Federal University of Technology, Akure, Ondo State, Nigeria*
[2] *Biomedical Engineering Unit, Federal Medical Centre, Ebute-Meta, Lagos State, Nigeria*

***Corresponding author:** vaakpan@futa.edu.ng

Original Research

Received:
23 May 2025

Revised:
21 September 2025

Accepted:
29 October 2025

Publish in Issue:
31 December 2025

Abstract

Chest diseases pose serious health threats if not detected early for properly and timely diagnosis. These diseases could include pulmonary disease, pneumonia, asthma, tuberculosis, lung diseases and other cardiovascular complications. When patients exhibit symptoms like chest pain, shortness of breath, or persistent cough; physicians often prescribe chest X-rays to assess the underlying cause of their discomfort. Chest X-ray is a commonly used diagnostic imaging test that requires significant expertise and careful observation to classify the particular or multiple chest diseases due to the complex nature of the pathology and fine texture of lung lesions. Chest X-Ray classification is a challenging and time consuming task in medical image classification due to the complexity of the human chest structure and the subtle variations in X-Ray images caused by different medical conditions. This paper presents a novel classification technique for the classification of 14 chest diseases that could impair patient's health. The classification technique presented in this paper is a deep convolutional neural network (CNN) algorithms based on DenseNet model structure for adaptive classification of chest diseases. This paper addresses and bridges three main research gaps in chest diseases classification, namely: 1). enhancing the classification accuracy and specificity in diagnosing up to 14 different classes of chest diseases based on label distributions; 2). develops an AI-based deep learning CNN using DenseNet model structure to accurately classify and predict the risk probability levels of heart failures based on chest X-ray images; and 3). the research leverages the issues of interpretability and explainability as the results is self-explanatory to clinicians. The results demonstrate the efficiency, proficiency and robustness of the deep CNN algorithm based on proposed DenseNet when compare to Inception and ResNet model structures. Additional justification of the DenseNet suitability has been validated with several standard performance metrics including saliency feature maps and DenseNet based Grad-CAM with LIME visualizations. The superior performance of the deep CNN based on the DenseNet model structure is further justified with standard performance metrics. The paper concludes with a comprehensive discussion on the DenseNet model's performance, shedding lights on its strengths and potential areas for improvement. The technique presented in this paper can easily be adapted for real-time chest diseases classification by clinicians.

Keywords: Chest Diseases Classification; Convolution neural Networks (CNN); Deep Learning; Deep Neural Network; DenseNet; X-Ray Images

Cite this article: Akpan, V. A. , Raji, N.O, Development of Deep Convolutional Neural Network Algorithms Based on Dense Net Model for Adaptive Classification of Chest Diseases. *Int. J. Biophoton. Biomed. Eng*. 2025;5(2): Article 9. doi.org/10.57647/ijbbe.2025.0502.09

1. Introduction

Chest X-ray diagnosis is a routine and crucial medical imaging procedure employed to generate images of the heart, lungs, blood vessels, airways, chest, and spine which plays a pivotal role in the detection and diagnosis of various lung and heart conditions [1,2]. When patients exhibit symptoms like chest pain, shortness of breath, or persistent cough, physicians often prescribe chest X-rays to assess the underlying cause of their discomfort. The significance of chest X-ray diagnosis lies in its capacity to provide valuable information about the patient's respiratory and cardiovascular health, aiding in the diagnosis of conditions such as pneumonia, emphysema, lung cancer, and lung collapse (pneumothorax) [1,2]. Additionally, chest X-rays can reveal heart-related lung problems, diagnose heart conditions like heart failure and fluid accumulation around the heart, visualize large blood vessels for the detection of aortic aneurysms or congenital heart diseases, identify bone issues, and fractures, and monitor postoperative changes after chest surgeries for recovery assessment, including heart, lung, or esophagus surgeries, checking for air leaks and fluid or air buildup [1–4].

Traditional diagnostic methods in healthcare have inherent limitations, leading to the need for more efficient and accurate approaches. Thus there is need to enhance the accuracy and efficiency of disease identification and classification in chest radiographs through the development of an artificial intelligence-based (AI-based) convolutional neural network (CNN) algorithms tailored for the adaptive classification of chest diseases based on X-ray images. AI-based CNN is a deep neural network scheme that is dedicated to image and video processing with an expected outcome of image classification, image recognition, pattern recognition, image segmentation, image identification, image localization [5–7]. AI-based CNN have proven successful in many applications [6–8] including medical image diagnosis [1–4,9,10]. Similar to shallow neural networks, deep neural networks requires a model structure; and there are over 22 pre-trained model structures for use with deep neural networks including AI-based CNN [11,12]. Among these pre-trained network models, VGG (visual geometry group) [13], ResNet (Residual network) [14], DenseNet (densely connected convolutional network) [15], Inception (Google network, GoogLeNet) [16], EfficientNet (efficient network) [17] and Ensemble Learning [13, 18, 19] have been used for chest disease classification [20, 21]. The just mentioned approaches for chest disease classification yielded successful results for only up to 5 chest parameters which may not be sufficient to capture the clinical conditions of the chest for proper diagnosis. This paper proposes the classification of 14 different chest parameters from a single chest X-ray image. The DenseNet pre-trained model structure is adopted in this research. Employing DenseNet, known for its dense connectivity and efficient parameter usage, the algorithm navigates through the intricacies of chest X-ray data, capturing intricate patterns and relationships within the images.

Chest X-ray diagnosis, while a common and valuable medical imaging procedure, presents certain limitations. Inter- and intraobserver variability introduces subjectivity in interpretation, impacting diagnostic consistency [22]. These X-rays may exhibit low sensitivity and specificity, contributing to false-negative or false-positive results and the potential for misdiagnosis. The detection of subclinical diseases, especially in high-income countries, poses a challenge, affecting early intervention strategies [23]. Additionally, the static nature of chest X-rays limits their ability to capture dynamic processes, hindering their efficacy in certain conditions. Furthermore, the requirement for specialized facilities may limit accessibility in various healthcare settings.

The interpretability and explainability of detections and classifications made by deep learning models pose challenges, impeding their widespread adoption in certain clinical settings. Some studies encounter limitations due to insufficiently annotated datasets, especially when investigating new and emerging diseases [24]. In the realm of chest X-ray image interpretation using deep learning, the consideration of additional clinical information is not consistently incorporated, potentially impacting diagnostic accuracy. While the potential of deep learning in chest disease diagnosis using chest X-ray images is evident from previous studies [25,26], there remains a need for further validation and testing to guarantee the reliability and generalization of these models. Addressing challenges associated with interpretability, dataset size, and model validation is crucial to ensure the successful integration of deep learning into clinical practice. This research attempt to address the above issues by evaluating the 14 available classes of chest diseases with sufficiently large different data set. A total of 112,120 frontal-view X-ray images of 30,805 unique patients, obtained from NIHCC [27], were used as training data set (80%) and validation data set (20%) while 108,948 frontal view X-ray images of 32,717 unique patients [28] were used for testing the AI-based CNN using the DenseNet pre-trained model structure.

The cardiovascular and respiratory systems are intricately linked, sharing a vital role in maintaining human health. The relationship between respiratory and cardiovascular diseases, and the impact of cardiovascular diseases on mortality in patients with respiratory disease is unclear [29]. Cardiovascular diseases encompass a range of conditions affecting the heart and blood vessels. Common examples include heart disease, cerebrovascular disease, and heart failure [30,31]. Respiratory disease conditions affecting the lungs and respiratory system, such as chronic obstructive pulmonary disease (COPD), pneumonia, and asthma, are

categorized as respiratory diseases [2,32,33]. Both categories of diseases often coexist, with studies showing a significant degree of co-morbidity, ranging from 17% to 35% in various groups [34]. Diagnosing and managing these diseases often requires an integrated approach due to shared symptoms and risk factors.

Early disease detection is vital in healthcare, offering benefits to individuals and the healthcare system. Timely identification enables targeted treatment, increasing the likelihood of success and potentially halting disease progression. This approach positively impacts patient survival rates, particularly in diseases like cancer, where early diagnosis improves treatment efficacy [2,32,33]. Additionally, early detection is cost-effective, reducing healthcare expenses by enabling less invasive interventions. It also enhances the quality of life for patients by preventing complications and improving overall well-being. Furthermore, early disease detection contributes to population health by allowing the timely implementation of preventive measures and interventions to control disease spread, benefiting the community as a whole.

For cardiovascular diseases, specific tests such as electrocardiograms (ECGs or EKGs), echocardiograms, or cardiac catheterization are commonly used for confirmation [29,35]. These tests offer more detailed information about the heart's function, structure, and blood flow [29,35]. Similarly, for respiratory diseases, additional tests such as pulmonary function tests, CT scans, or MRIs may be needed to confirm a diagnosis [24]. Chest X-rays can identify certain respiratory conditions, but might not provide sufficient detail for a conclusive diagnosis. Issues such as limited sensitivity and specificity, resulting in false-negative or false-positive results, can lead to misdiagnosis and impact patient outcomes. The reliance on subjective interpretation by healthcare professionals introduces variability and inconsistency in diagnoses, influenced by differences in expertise and experience [24,36,37]. Moreover, some traditional methods requiring specialized facilities may pose challenges in resource-limited or remote healthcare settings, hindering timely and accurate diagnoses.

To address these challenges, there is a growing interest in advanced technologies such as incorporating artificial intelligence (AI) and deep learning CNN. These AI-based CNN technologies, when coupled with large datasets and imaging techniques, offer improved objectivity, accuracy, reduced variability, and faster results for medical image interpretation [38]. Integrating AI-based deep learning CNN advancements into clinical practice can lead to more precise and data-driven diagnostic tools, ultimately enhancing patient outcomes and optimizing healthcare resources. Chest X-rays are pivotal in diagnosing heart disease by offering a comprehensive view of chest structures, particularly the heart. They enable the identification of cardiovascular abnormalities, such as cardiomegaly, providing crucial insights into heart size and shape. In cases of congestive heart failure, chest X-rays are instrumental in detecting signs like pulmonary edema, facilitating timely diagnosis and management [39]. Chest X-rays also contribute to evaluating blood vessels, aiding in the assessment of conditions like aortic aneurysms [2,20]. Furthermore, chest X-ray images have the abilities to reveal lung conditions impacting the heart, such as pneumonia or pleural effusion, underscores their significance in the comprehensive evaluation of cardiac health [1–3]. Beyond diagnosis, chest X-rays play a vital role in monitoring treatment responses and guiding further investigations based on identified abnormalities [20,40]. On the overall, chest X-ray images serve as a foundational and non-invasive diagnostic tool for assessing heart health, supporting the identification, diagnosis, and monitoring of diverse cardiovascular conditions [36,41]. However, thoughtful consideration of ethical aspects, data privacy, and the continued importance of human expertise is crucial in implementing AI-based deep learning CNN technologies in healthcare diagnostics. Chest diseases that may arise from the careful examination of the chest can be classified as: 1). Cardiomegaly [42], 2). emphysema [43], 3). Effusion [44], 4). hernia [45], 2023), 5). Infiltration [46], 6). Mass [47], 7). Nodule [48], 8). Atelectasis [49], 9). Pneumothorax [50], 10). Pleural thickening [44], 11). Pneumonia [51], 12). Fibrosis [52], 13). Edema [39], and 14). Consolidation [53]. The development of a AI-based deep learning CNN model for accurate detection and classification of the 14 different classes of chest diseases from chest X-rays will offer significant benefits in clinical practice and patient care. Such benefits will include high-precision disease detection, improving diagnostic efficiency by providing automated analysis, enhancing resource allocation for prioritized treatment, and serving as a decision-support system (DSS) for clinicians [10]. The model’s ability to identify diseases early, such as early-stage lung cancers and pneumonia will contribute to effective treatment and improved patient outcomes. In summary, the AI-based deep learning CNN based the DenseNet model have the transformative potential, providing accurate disease detection, classification aiding clinical decision-making, enabling early intervention, and optimizing healthcare resource allocation.

2. Related works

Deep learning architectures have shown remarkable advancements in medical image analysis, particularly in the context of chest X-ray diagnosis [11,13,16,18]. These deep learning architectures leverage convolutional neural networks (CNNs) and other deep learning techniques to achieve state-of-the-art performance in various tasks related to chest radiography. They have the potential to assist medical professionals in early diagnosis, enabling timely and effective treatment. With the availability of large chest X-ray datasets and the continuous advancement of deep learning techniques, the future of chest X-ray diagnosis looks promising, with the potential for further improvement in performance and clinical applications.

In 2023, Nasser and Akhloufi discussed multiple publicly available chest X-ray datasets for different diseases and presents an overview of recent deep

learning models used for chest disease detection [21]. The study highlights various deep learning architectures, including VGG, ResNet, DenseNet, Inception, EfficientNet, RetinaNet, and ensemble learning methods. Techniques for chest X-ray (CXR) image preprocessing, such as enhancement, segmentation, bone suppression, and data augmentation, are also explored. The key emphasizes is on the importance of interpretability and explainability to better understand the deep learning model detections [21].

Another survey reviewed and technically evaluated different computer-aided chest pathologies detection systems based on deep learning. The study covered single and multi-pathologies detection systems published in the last five years. The paper discussed the taxonomy of image acquisition, dataset preprocessing, feature extraction, and deep learning models used. The article compared various articles based on their contributions, datasets, methods, and results achieved [54].

The evolution of chest radiography and fluoroscopy since Wilhelm Rontgen's discovery of X-rays has been examined [55]. Emphasis on the use of CXR as a first-line imaging tool for chest assessment worldwide was discussed. Recent evidences for using modern machine learning to improve the efficiency and accuracy of CXR interpretation was highlighted. While acknowledging the potential of machine learning algorithms, the study also mentions the current limitations of these algorithms in providing comprehensive assessment and considering relevant clinical information [55].

Iqbal and co-workers attempted to address the challenge of handling imbalanced datasets, particularly in the context of viral epidemics, where limited annotated data is available for lung disease signs from chest X-ray and CT images [36]. The proposed technique, called 3-Phase Dynamic Learning (3PDL), utilizes deep learning and Support Vector Machine (SVM) for image classification. The approach achieves high F1 scores and precision, indicating its potential as a pathologist's assistive tool [24,36].

While deep learning techniques have exhibited promise in classifying chest X-ray images for COVID-19 and other lung diseases, several gaps persist in the existing literature. [1,4,13,19,56,57]. Many studies report high accuracy in classifying COVID-19 patients from normal or other pneumonia cases, but these results often arise from cross-validation studies without an independent test set, potentially introducing biases and overfitting issues [1,4,13,19,56–58]. The challenge of imbalanced datasets, where one class significantly outweighs the other, can impact model performance negatively, especially in chest X-ray diagnosis, where there might be an unequal distribution of COVID-19 positive cases compared to normal or other lung diseases [1,4,24,36,56,59]. Addressing class imbalance is crucial to prevent biased model predictions and ensure accurate detection across all classes. Transfer learning, a strategy involving pre-trained models on larger datasets, is employed to mitigate the challenge of obtaining labeled medical images for training, but optimal model selection and fine-tuning for chest X-ray diagnosis remain active areas of research [4,40,56,60]. Moreover, the "black box" nature of deep learning models in medical settings necessitates efforts to enhance explainability for gaining the trust of healthcare practitioners, prompting ongoing research in methods to interpret and explain the decisions made by these models in chest X-ray diagnosis [24].

The literature review on chest X-ray diagnosis using deep learning reveals significant findings [4,9,21]. AI-based deep learning models exhibit effectiveness in classifying chest X-ray images for various diseases, including COVID-19, pneumonia, and other lung diseases [1,2,4,19]. The success of these models is contingent on a sufficiently large training dataset, and techniques such as data augmentation [61] and generative adversarial networks (GANs) [62] have been employed to address challenges posed by small datasets with little model improved performance [57]. Transfer learning has further been leveraged to improve feature extraction for chest X-ray image classification [60]. In addition, hyperparameter tuning has proven valuable by achieving accuracies consistently higher than 97%. [4,40,60]. The current project aims to address three research gaps, namely: 1). enhancing the classification accuracy and specificity in diagnosing up to 14 different classes of chest diseases; 2). develope an AI-based deep learning CNN using DenseNet model to classify and predict the risk level of heart failure based on chest X-ray images; and 3). the research will leverages the issues of interpretability and explainability as the results will be self-explanatory to the clinicians.

3. Background knowledge

3.1. Convolutional Neural Networks (CNN)

Convolutional neural networks (CNN) are specialized deep neural network algorithms designed for processing grid-like data such as images. CNN are designed for task that require object recognition including image classification, detection, segmentation and localization [5–8]. In a typical CNN model, the input image in the form of data is passed through a series of layers that are designed to extract features and consequently perform the classification of the extracted features to produce a label for the input image. The architecture of a convolutional neural network model is shown in Figure 1.

The basic building blocks of a CNN are convolutional layers which use convolutional filters to extract features from the input data, and the padding and pooling layers which down sample the output of the convolutional layers to reduce the dimensionality of the data. After passing through several convolutional, padding and pooling layers, the output is flattened and fed into a series of fully connected layers which performs classification or regression on the extracted features to produce a label for the input image. Generally, the CNN model has two main parts, namely: i). Feature extraction and ii). Classification.

10.57647/ijbbe.2025.0502.09

1) Feature Extraction

Feature extraction involves the techniques that are used to automatically and efficiently extract the spatial features from input images and make the machine to learn those features automatically. In CNN, the feature extraction is influenced by five major components, namely: convolution layer, stride, padding, activation function and pooling layer which are briefly described in the following.

a) Convolution Layer

The convolution layer is specifically used for feature extraction. The convolution layer is the first building block of a CNN. As the name suggests, the main mathematical task performed is called convolution, which is the application of a sliding window function to a matrix of pixels representing an image. The sliding functions applied to the matrix are small grids called kernels or convolution filters.

In the convolution layer, several convolution filters of equal size are applied, and each convolution filter is used to recognize a specific pattern from the image, such as the curving of the digits, the edges, the whole shape of the digits, and more. In fact, in the convolution layer, the small grids (kernels or convolution filters) move over the image and checks for specific patterns in the image and highlights such pattern. By using several different convolution filters, the CNN can get a good idea of all the different patterns inherent in the image. Put simply, in the convolution layer, we use small grids (called filters or kernels) that move over the image. Each small grid is like a mini magnifying glass that looks for specific patterns in the photo, like lines, curves, or shapes. As it moves across the photo, it creates a new grid that highlights where it found these patterns. Detailed and complete treatment of CNN with associated pre-trained models can be found in [5–8, 11,12, 63, 64].

3.2. Classified chest diseases

Different from all the literature reviewed, this research has been able to identify 14 different classed of chest diseases that have potential life-threatening effects on a patient. It should be noted Figure 2 depicts the X-ray image of a normal healthy chest where the risk level will be approximately zero. The description of these 14 different classes of chest diseases considered in this research (shown in Figure 3 to Figure 16) are briefly discussed below:

(i) Cardiomegaly*:* Cardiomegaly, also known as an enlarged heart, is a medical condition characterized by an increase in the size of the heart. It is a symptom or a manifestation of an underlying medical condition. The Chest x-ray for Cardiomegaly is shown in Figure 3. Cardiomegaly can occur in response to various factors, and its presence often indicates an issue with the heart's structure or function. It refers to the enlargement of the heart, typically due to chronic conditions such as hypertension, heart valve disease, or cardiomyopathy [42].

(ii) Emphysema*:* Emphysema is a chronic obstructive pulmonary disease (COPD) characterized by the gradual destruction of lung tissue, primarily caused by smoking or long-term exposure to pollutants. It is a chronic and progressive lung disease that primarily affects the alveoli, which are tiny air sacs in the lungs responsible for gas exchange. It falls under the broader category of chronic obstructive pulmonary disease (COPD), along with chronic bronchitis. The Chest x-ray for Emphysema is shown in Figure 4. Emphysema is characterized by the gradual destruction of the alveolar walls, leading to decreased lung function and difficulty in breathing [43].

(iii) Effusion: Effusion refers to the abnormal accumulation of fluid in body cavities particularly within the chest (thoracic cavity) or around the lungs. This condition can lead to various symptoms and may indicate an underlying medical issue [44].The Chest x-ray for Effusion is shown in Figure 5.

(iv) Hernia: Hernia is the protrusion of an organ or tissue through an abnormal opening in the body. It is a medical condition that occurs when an organ or tissue pushes through a weak spot or opening in the surrounding muscle or connective tissue that holds it in place. This can result in a noticeable bulge or lump that can often be seen or felt. Hernias can develop in various parts of the body, but they are most commonly found in the abdomen [45]. The Chest x-ray for Hernia is shown in Figure 6.

(v) Infiltration: Infiltration is a broad medical term that refers to the process by which foreign substances or abnormal cells enter and accumulate within a tissue, organ, or body space. In the context of chest diseases, infiltration can have various underlying causes and implications. The Chest x-ray for Infiltration is shown in Figure 7. It is important to note that “infiltration” itself is not a specific disease but rather a descriptive term that can be associated with different conditions [46].

(vi) Mass: A mass in the context of chest disease refers to an abnormal growth or lump in the lung or surrounding tissues, which can be benign or malignant. "Chest mass" is a general term that refers to the presence of an abnormal lump or growth in the chest area. The Chest x-ray for Mass is shown in Figure 8. Chest masses can arise from a variety of underlying causes, some of which may be benign (non-cancerous) and others that could be malignant (cancerous) [47].

(vii) Nodule: A lung nodule is a small, rounded lesion or spot in the lung, often detected incidentally in imaging studies. Nodule is a term used in medicine to describe a small, solid, rounded growth or lump that can form in various tissues or organs within the body. Nodules can develop for a variety of reasons, and their significance can vary greatly depending on their location, size, and underlying cause [48]. The Chest x-ray for Nodule is shown in Figure 9.

(viii) Atelectasis: Atelectasis is the partial or complete collapse of a lung or part of a lung due to blocked air passages. Atelectasis is a medical term that refers to a

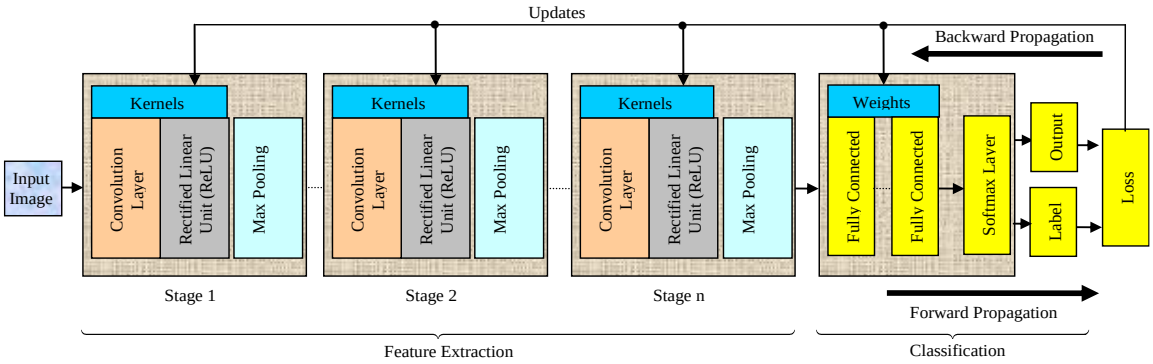

Figure 1. Convolution neural network model architecture

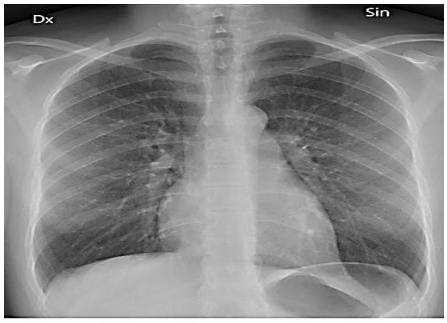

Figure 2. Normal Chest X-ray

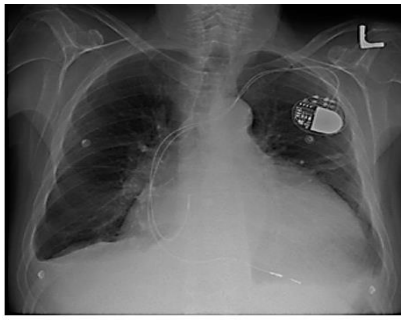

Figure 3. Cardiomegaly Chest X-ray

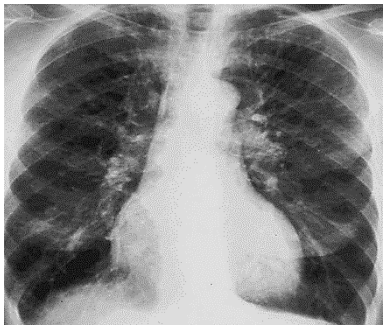

Figure 4. Emphysema Chest X-ray

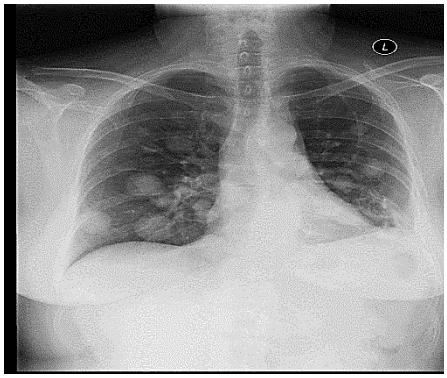

Figure 5. Effusion Chest X-ray

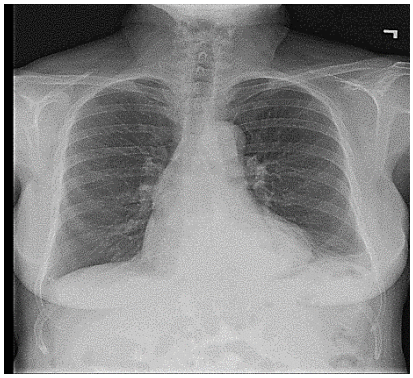

Figure 6. Hernia Chest X-ray

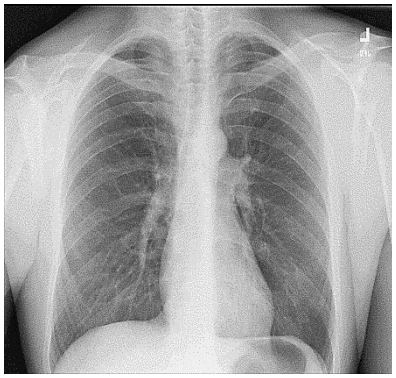

Figure 7. Infiltration Chest X-ray

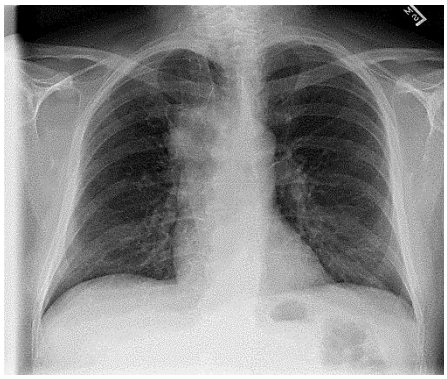

Figure 8. Mass Chest X-ray

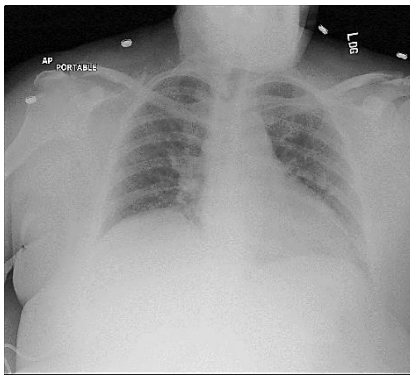

Figure 9. Nodule Chest X-ray

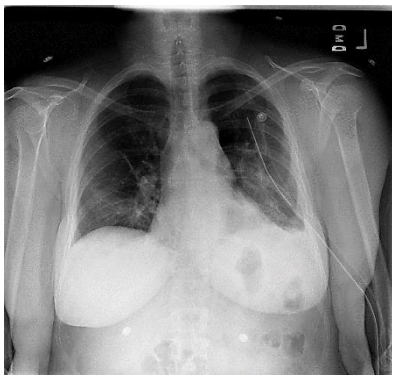

Figure 10. Atelectasis Chest X-ray

10.57647/ijbbe.2025.0502.09

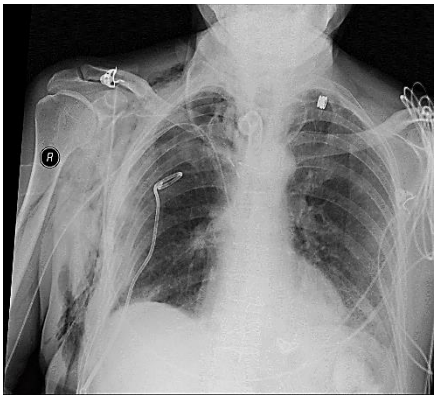

Figure 11. Pneumothorax Chest X-ray

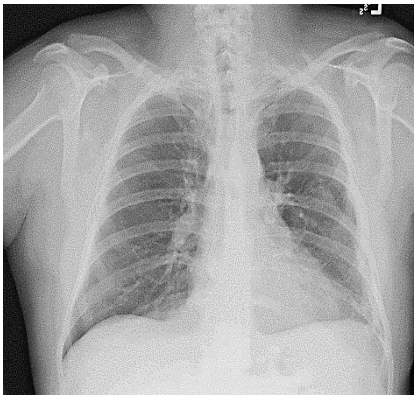

Figure 12. Pleural thickening Chest X-ray

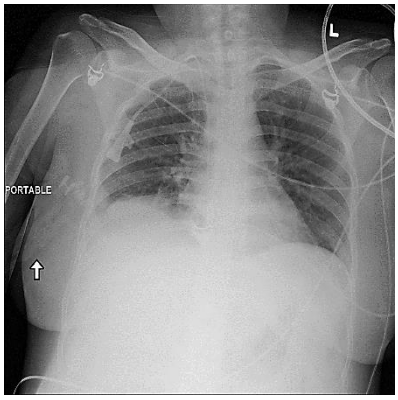

Figure 13. Pneumonia Chest X-ray

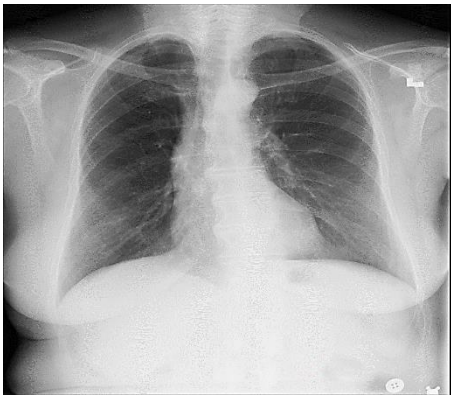

Figure 14. Fibrosis Chest X-ray

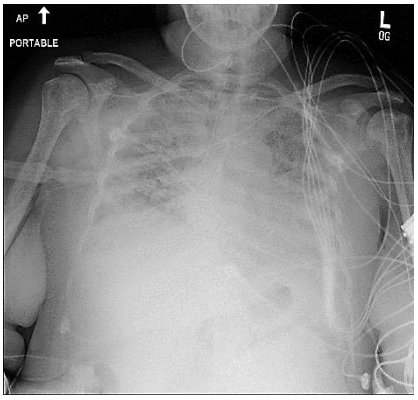

Figure 15. Edema Chest X-ray

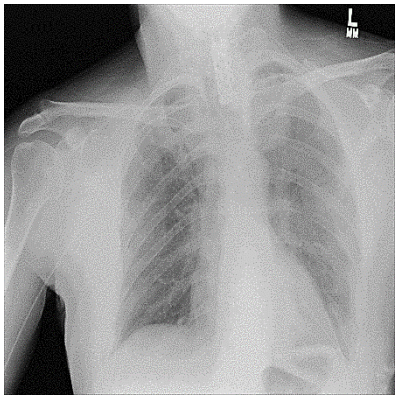

Figure 16. Consolidation Chest X-ray

partial or complete collapse of a lung or a portion of a lung. This condition occurs when the tiny air sacs in the lung, called alveoli, deflate and cause the lung tissue to collapse. The Chest x-ray for Atelectasis is shown in Figure 10. Atelectasis can affect people of all ages and can vary in severity, from a small area of lung collapse to an entire lung lobe [49].

(ix) Pneumothorax: Pneumothorax is the presence of air in the pleural space between the lung and the chest wall, leading to lung collapse. Pneumothorax is a medical condition that affects the lungs and chest cavity. It occurs when air accumulates in the pleural space, which is the space between the lung and the chest wall. This buildup of air can lead to lung collapse, causing a variety of symptoms and potential complications [50]. The Chest x-ray for Pneumothorax is shown in Figure 11.

(x) Pleural Thickening: Pleural thickening is the scarring and thickening of the pleura, the membranes surrounding the lungs. Pleural thickening is a medical condition that affects the pleura, which is the thin, double-layered membrane that surrounds the lungs and lines the inside of the chest cavity. The Chest x-ray for Pleural thickening is shown in Figure 12. Pleural thickening occurs when the pleura becomes abnormally thickened and scarred, often as a result of prolonged inflammation or irritation. This condition can lead to a range of symptoms and potential complications [44].

(xi) Pneumonia: Pneumonia is an infection that causes inflammation in the air sacs of the lungs, affecting lung function. Pneumonia is a common and potentially serious chest disease that affects the lungs. It is characterized by inflammation and infection of the air sacs in one or both lungs, which can cause a range of symptoms and complications. Pneumonia can affect people of all ages, but it is more dangerous for young children, the elderly, and individuals with weakened immune systems [51]. The Chest x-ray for Pneumothorax is shown in Figure 13.

(xii) Fibrosis: Fibrosis is a condition in which lung tissue becomes scarred and thickened over time. Fibrosis is a medical condition characterized by the excessive accumulation of fibrous connective tissue in an organ or tissue, leading to scarring and functional impairment. It is a common response to injury or inflammation and can occur in various organs throughout the body. The Chest x-ray for Fibrosis is shown in Figure 14. Fibrosis can have serious consequences, as it can disrupt the normal structure and function of affected tissues and organs [52].

(xiii) Edema: Edema is the accumulation of fluid in the lung tissue and air sacs, impairing oxygen exchange. Edema is a medical term used to describe the abnormal accumulation of fluid in the interstitial spaces within body tissues, leading to swelling. It can occur in various parts of the body and is often a sign of an underlying medical condition. Edema can affect any age group and may be acute (short-term) or chronic (long-term). It's important to note that edema itself is not a disease but a symptom of an underlying problem [39]. The Chest x-ray for Edema is shown in Figure 15.

(xiv) Consolidation: Consolidation is the replacement of normal air-filled lung tissue with fluid or other substances. Consolidation is a medical term used to describe a specific type of chest disease that involves the

filling of the air sacs (alveoli) in the lungs with fluid, pus, blood cells, and other substances, causing them to become solid and less able to function properly. The Chest X-ray for Consolidation is shown in Figure 16. This condition is often associated with various respiratory illnesses, most notably pneumonia. It results in decreased gas exchange within the affected lung tissue, leading to impaired oxygenation of the blood [53].

4. Development of the cnn algorithm based on densenet model

4.1. Materials and technologies

The materials employed in this research are: *(i)* Google Colaboratory cloud-based code editor; *(ii)* T4 Graphical Processing Unit (GPU); *(iii)* Python software and associated libraries*; (iv)* Tensorflow, Keras, Numpy, Pandas, Seaborn and Matplotlib Libraries; *(v)* a high speed Internet connection; and *(vi)*108 frontal view X-ray images of 32,717 unique patients. A total of 112,120 frontal-view X-ray images of 30,805 unique patients, obtained from NIHCC [27], were used as training data set (80%) and validation data set (20%) while 108,948 frontal view X-ray images of 32,717 unique patients [28] were used for testing the AI-based CNN using the DenseNet pre-trained model structure. After the data set pre-processing, a total of 141,537 class label distributions on the data set were obtained as listed in Table 1 for each class of the chest disease to facilitate the chest X-ray disease classification. There is no patient overlap between the data sets.

4.2. Dense Convolutional Neural Network (DenseNet)

4.2.1 *Dense Convolutional Neural Network (DenseNet)*

DenseNet's densely connected architecture ensures that each layer receives direct input from all preceding layers and passes its own feature maps to all subsequent layers. This promotes extensive feature reuse, allowing for a more efficient flow of information through the network. Huang and co-workers stated in their original DenseNet paper that this connectivity pattern encourages feature propagation and leads to improved parameter efficiency [66].

The use of dense connections enables the gradient to flow directly through the network, mitigating the vanishing gradient problem. This makes it feasible to train very deep networks, which is a significant advantage in tasks In tasks that require complex feature hierarchies. It also reduces the number of parameters compared to traditional architectures like popular AlexNet by eliminating the need for separate learned features at each layer. This leads to a more parameter-efficient model, which is crucial for applications with limited computational resources.

The paper by Huang and co-workers demonstrated through experiments that DenseNet achieves competitive or better performance with fewer parameters compared to other pre-trained model structures [66]. DenseNet's densely connected blocks are highly effective for tasks like image segmentation, where precise labeling of pixels is essential. The architecture's ability to capture fine-grained features across multiple scales makes it particularly well-suited for such tasks.

The choice of DenseNet for the project is grounded in its ability to facilitate efficient information flow, mitigate gradient vanishing, utilize parameters effectively, and excel in tasks like image segmentation.

DenseNet introduces densely connected layers where each layer receives input from all preceding layers [15,66]. A DenseNet is a type of convolutional neural network that utilizes dense connections between layers, through Dense Blocks, where we connect *all layers* (with matching feature-map sizes) directly with each other. To preserve the feed-forward nature, each layer obtains additional inputs from all preceding layers and passes on its own feature-maps to all subsequent layers. This fosters feature reuse and reduces the risk of vanishing gradients. The DenseNet architecture is shown in Figure 17 and was developed specifically to improve the declined accuracy caused by the vanishing gradient in high-level neural networks. In simpler terms, due to the longer path between the input layer and the output layer, the information vanishes before reaching its destination. The key characteristics of the DenseNet are: *(i) Dense Blocks*: Each layer receives feature maps from all preceding layers and passes its own feature maps to all subsequent layers; *(ii) Transition Layers:* These layers control the growth of feature maps and reduce spatial dimensions; and *(iii) Applications include Image Segmentation*: DenseNet is highly effective in tasks like image segmentation, where it can precisely label pixels in an image.

4.2.2 *The DenseNet CNN-Based algorithm*

According to the discussion of Section III(A) based on Figure 1, the deep CNN is trained firstly with a forward

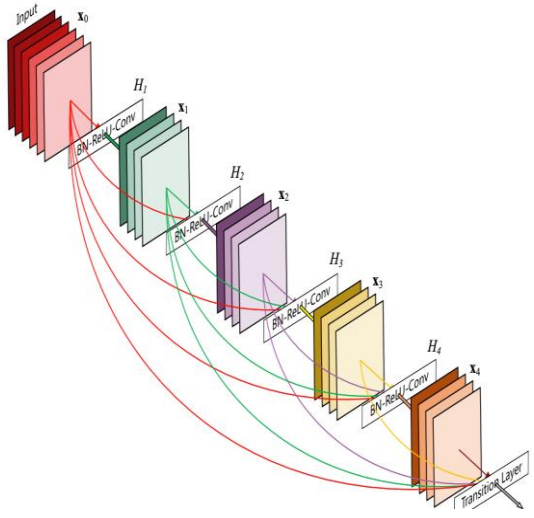

Figure 17. DenseNet Architecture

propagation algorithm for weights and bias adjustments followed by a backward propagation for weights and bias corrections for accurate classification of the output image based on the extracted features of the input images. In the following, the forward and backward propagation algorithms are presented.

4.2.2.1 *Forward propagation*

1. *Dense connectivity:*

The DenseNet-121 comprises 4 dense blocks, which themselves comprise 6 to 24 dense layers. A dense block comprises n dense layers. These dense layers are connected such that each dense layer receives feature maps from all preceding layers and passes its feature maps to all subsequent layers. The dimensions of the feature maps (width, height) stay the same in a dense block.

Given input X_i to a layer in a dense block, the output is computed by concatenating the feature maps from all preceding layers: $X_i = [X_0, X_1, \ldots, X_{i-1}]$. The input layer to the DenseNet is an image tensor X with dimension $320*320*1$, representing a $320*320$ image with one color channels (grayscale).

$$X = \begin{bmatrix} X_{11} & X_{12} & \cdots & X_{1m} \\ X_{21} & X_{22} & \cdots & X_{2m} \\ \vdots & \vdots & \ddots & \vdots \\ X_{m1} & X_{m2} & \cdots & X_{mm} \end{bmatrix} \quad (1)$$

The weight associated with each feature are represented by *W*.

$$W = \left[w_1, w_2, \ldots, w_n\right] \quad (2)$$

The output H_i is passed through a series of convolutional and batch normalization operations.

2. *Dense layer:*

Each dense-layer consists of 2 convolutional operations, namely:
(i) 1×1 CONV (conventional convolution operation for extracting features)

(ii) 3×3 CONV (bringing down the feature depth/channel count)

The CONV layer corresponds to the sequence BatchNorm $\rightarrow$ ReLU $\rightarrow$ Conv. A layer has each sequence repeated twice, the first with 1×1 Convolution bottleneck producing: growth rate x 4 feature maps, the second with 3x3 convolution. The growth rate ($k = 32$ for DenseNet-121) defines the number of output feature maps of a layer [15,66]. Basically the layers output 32 feature maps which are added to a number of 32 feature maps from previous layers. While the depth increases continuously, each layer bring back the depth to 32.

The convolutional layer applies filters (W_c) to the input image, producing feature maps and the bias (b_c) are added to the result of the convolution (see Section III(A) for detailed background knowledge on CNN).

3. *Convolution operation:*

$$\left.\begin{array}{l} \textit{for } l = 1 \textit{ to } l-1: \\ \quad Z^{(l)} = W^{(l)} A^{(l-1)} + b^{(l)} \\ \quad A^{(l)} = g^{(l)} * Z^{(l)} \\ \textit{end} \end{array}\right\} \quad (3)$$

where $W^{(l)}$ Represents the weight matrix of the l^{th} layer, $A^{(l-1)}$ is the output (activation) of the $((l-1)^{th}$ layer, $b^{(l)}$ is the bias vector of the l^{th} layer, and g^{th} is the activation function applied element-wise to $Z^{(l)}$. Also, the *W* is the convolutional filter (weights), *b* denote the bias and * denotes the convolution operation.

4. *Transition layer:*

After each dense block, a transition layer is used to reduce dimensions. If X_i is the input, then

$$\left.\begin{array}{l} H_{i+1} = \text{Conv2D}\left(\text{X}_i\right) + \text{BatchNorm}\left(\text{X}_i\right) \\ \qquad + \text{ReLU}\left(\text{X}_i\right) + \text{AveragePooling}\left(\text{X}_i\right) \end{array}\right\} \quad (4)$$

5. *Global average pooling:*

After the last dense block, global average pooling is applied:

$$\text{H}_{\text{GAP}} = \text{GlobalAveragePooling}\left(\text{H}_{\text{last}}\right) \quad (5)$$

6. Final classification layer:

The output of GAP is connected to the final dense layer with sigmoid activation for classification. The last layer of the model is a Dense layer with a sigmoid activation function, which is commonly used for binary classification problems. The sigmoid function squashes the output values between 0 and 1, making it suitable for binary predictions. Let $Z^{[L]}$ be the input to the last layer, where L is the index of the last layer. The output $A^{[L]}$ is computed as follows:

$$z^{(l)} = W^{(l)} A^{(l-1)} + b^{(i)} \quad (6)$$

$$\hat{y} = g^{(l)} * z^{(l)} \quad (7)$$

where $\hat{y}$ is the predicted output of the neural network. Introducing additional elements and regularization terms, we have

$$\left.\begin{array}{l}\text{Cross}-\text{Entropy Loss}:\\ L(\hat{y},y)=-\left(y*\log(\hat{y})+(1-y)\log(1-\hat{y})\right)\end{array}\right\} \quad (8)$$

where y is the ground truth labels; Dropout: $D^{(l)}$ is applied to $A^{(l)}$; and Batch Normalization: $BN^{(l)}$ is applied to $Z^{(l)}$.

The variable $z^{(l)}$ is often referred to as the weighted input to the activation function in the l^{th} layer. Its purpose is to capture the linear combination of the inputs from the previous layer, weighted by the synaptic weights, and includes the bias term. Where $W^{(l)}$ represents the weight matrix of the l^{th} layer, $A^{(l-1)}$ is the output (activation) of the $(l-1)^{th}$ layer, $b^{(l)}$ is the bias vector of the l^{th} layer, and $Z^{(l)}$ is the total weighted input.

The weighted input $z^{(l)}$ is then passed through an activation function $g^{(l)}$ to introduce non-linearity into the model:

$$A^{(l)}=g^{(l)}*Z^{(l)} \quad (9)$$

4.2.2.2. *Backward propagation (gradient descent) Back-propagation through dense blocks and transition layers*

Gradients are computed with respect to the loss and propagated backward through each layer. The general formula for computing the gradient, often referred to as back-propagation, involves applying the chain rule of calculus. The gradient of the loss with respect to the parameters can be expressed as follows:

1. Output layer (Layer L):

$$\left.\begin{array}{c}\delta^{(l)}=\dfrac{\partial l}{\partial Z^{(l)}}\\ \dfrac{\partial l}{\partial W^{(l)}}=\delta^{(l)}\cdot(A^{(l-1)})^{T}\\ \dfrac{\partial l}{\partial b^{(l)}}=\sum\delta^{(l)}\end{array}\right\} \quad (10)$$

2. Hidden layers to $(l=L\text{-}1\ to\ 1)$:

$$\left.\begin{array}{l}for\ l=L-1\ to\ 1:\\ \delta^{(l)}=\left(\left((W^{l+1})\cdot\delta^{(l+1)}\right)\odot^{*}\dot{g}^{(l)}(z^{(l)})\right.\\ \dfrac{\partial l}{\partial W^{(l)}}=\delta^{(l)}\cdot\left(A^{(l-1)}\right)^{T}\\ \dfrac{\partial l}{\partial b^{(l)}}=\sum\delta^{(l)}\end{array}\right\} \quad (11)$$

Table 1. Details of DenseNet architectural parameters

Layer(type)	Output Shape	Parameters
Input Layer	(None, None, None, 3)	
Convolutional Blocks	(None, None, None, 3)	36864
Pooling Layers	(None, None, None, 5)	524288
Concatenation Layers	(None, None, None, 1)	4096
Batch Normalization	(None, None, None, 1)	4096
ReLu(activation)	(None, None, None, 1)	0
Global Average Pooling	(None, 1024)	0
Fully connected layers(Dense)	(None, 14)	14350
Total Parameters	: 7,051,854	
Trainable Parameters	: 6,968,206	
Non-trainable Parameters	: 83,648	

where * denote element-wise multiplication, $\dot{g}^{(l)}$ is the derivative of the activation function $g^{(l)}$ with respect to its input.

3. Regularization Terms: The regularization terms are given as

$$\frac{\partial R\left(W^{(l)}\right)}{\partial W^{(l)}} \quad and \quad \frac{\partial R\left(A^{(l-1)}\right)}{\partial A^{(l-1)}} \quad (12)$$

4. Binary Accuracy: Binary accuracy is the ratio of correct predictions to the total number of predictions

$$\left.\begin{array}{l}\text{Binary Accuracy}\\ =\dfrac{Number\ of\ correct\ predictions}{Total\ Number\ of\ predictions}\\ =\dfrac{TP+TN}{TP+TN+FP+FN}\end{array}\right\} \quad (13)$$

5. Precision Equation: Precision is the ratio of true positive predictions to the total predicted positives

$$\text{Precision}=\frac{TP}{TP+FP} \quad (14)$$

6. Recall (sensitivity or True Positive Rate):

Recall is the ratio of true positive predictions to the total actual positives.

$$\text{Recall}=\frac{TP}{TP+FN} \quad (15)$$

10.57647/ijbbe.2025.0502.09

where TP (True Positives), TN (True Negatives), FP (False Positives), FN (False Negatives) for precision and recall. These metrics is computed using the predicted outputs ($\hat{y}$) and the actual labels (y) after model training.

7. F1-Score: The F1-score is the harmonic mean of precision and recall. The F1-score will be used to provide a balanced measure of model performance. This metric is useful to handle the imbalance in class distribution and is especially relevant for cases where certain classes may dominate the dataset. The F1-score is calculated as:

$$F1\ Score = 2 \times \frac{Precision \times Recall}{Precision + Recall} \tag{16}$$

This metric is particularly important in situations where both precision and recall are important, as it balances the trade-off between them.

8. AUC-ROC: The area under receiver operating characteristic curve (AUC-ROC) is mathematically described as the integral of the True Positive Rate (TPR) with respect to the False Positive Rate (FPR) across all possible classification thresholds, and can be interpreted as the probability that a randomly chosen positive instance will be ranked higher than a randomly chosen negative instance. It quantifies the performance of a binary classifier across its entire range of operating points, with values closer to 1 indicating better performance. AUC-ROC can be expressed mathematically as:

$$\left.\begin{aligned} AUC - ROC &= \int_0^1 TPR\left(FPR\right) dFPR \\ &= \int_0^1 TPR\left(FPR^{-1}\left(x\right)\right) dx \end{aligned}\right\} \tag{17}$$

9. Confusion Matrix: A confusion matrix does not have a single formula but is a table used to summarize the performance of a classification model by showing the actual versus predicted classes. For a two-class problem, it includes four components: True Positives (TP), True Negatives (TN), False Positives (FP), and False Negatives (FN). These components are then used in formulas to calculate performance metrics such as the Accuracy (as defined in (13)), Precision (Positive Predictive Value, PPV given in (14), Recall (Sensitivity, True Positive Rate defined in (15)), Specificity (True Negative Rate), and the F1 score (given by (16)).

4.2.3. *The complete developed densenet CNN architecture*

DenseNet121 is a CNN architecture tailored for detection of 14 different pathologies from chest X-ray images. It is based on DenseNet CNN architecture. DenseNet stands for Densely Connected Convolutional Network and it has 121 layers deep CNN architecture pre-trained on ImageNet dataset. In DenseNet, each layer is densely connected to every other layer in a feed-forward fashion. This means that the output of each layer is fed directly as input to all subsequent layers. This dense connectivity pattern encourages feature reuse and allows for efficient learning and propagation of information through the network. Specifically, in DenseNet architecture, the input of a layer is the concatenation of the feature maps from all preceding layers. This dense connectivity enables efficient learning and parameter reduction compared to traditional architectures. It also helps mitigate the vanishing gradient problem and facilitates feature propagation.

DenseNet operates on the principle of densely connected layers throughout the network, promoting efficient feature reuse and propagation. DenseNet has 7,051,854 parameters in total out of which 6,968,206 are trainable and 83,648 are non-trainable parameters. Architecture details, layer-wise parameters and output shape of DenseNet121 mode are shown in Table 1. To initialize the model parameters, Transfer Learning techniques described in [4,36,60] combine with the techniques discussed in Section III(A)(3) were used to overcome the problem of over-fitting. All the layers discussed above are stacked up to make a full CNN architecture. In addition to these main layers mentioned above, CNN also include optional layers like batch normalization layer to improve the training time and dropout layer to address the over-fitting issue (see Section III(A)(3)). The CNN Algorithmic model based on DenseNet model structure is shown in Figure 18.

4.3. Quantitative benchmarking criterion for the proposed CNN with densenet model structure

4.3.1. *InceptionV3 and ResNet Model Structures*

In other to evaluate the performance of the proposed deep CNN based on DenseNet model structure, it is imperative to compare its performance with two widely used model structures for CXR classification, namely: InceptionV3 [11, 16, 67–70] and ResNet [11,14,68–72]. The complete description of these model structures can be found in [5–7,11].

4.3.1.1. *The InceptionV3*

The InceptionV3 model architecture for chest X-ray classification uses its core design of parallel convolutional layers within Inception modules to efficiently capture multi-scale features from the X-rays [5,8,16]. This deep convolutional neural network (CNN), pre-trained on large datasets like ImageNet, is adapted for medical imaging through a process called transfer learning to classify diseases such as pneumonia or COVID-19 from chest X-ray images [68–70]. The standard InceptionV3 model serves as a feature extractor, often followed by dense layers and a softmax classifier to output the final diagnosis [11,68–70].

4.3.1.2. *ResNet-50*

The ResNet-50 architecture, a 50 layer CNN, is widely used for chest disease classification from X-ray images

by leveraging transfer learning and fine-tuning pre-trained models [11, 14, 68–72]. Its key feature is residual connections, which help prevent the vanishing gradient problem and enable the network to effectively extract deep features from complex medical images for accurate disease detection, such as pneumonia or COVID-19 [68–73].

4.3.2. *Interpretability via visualizations criterions*

4.3.2.1. *Salience, ICA and feature maps*

A saliency map shows which parts of an input (like an image) are most important for a model's decision, while a feature map shows the output of a specific filter in a neural network, highlighting features like lines or curves [70,72]. An Independent Component Analysis (ICA) saliency map is a specific type of saliency map that uses ICA to identify and emphasize salient features or regions in the data. A saliency feature map is a broad term for any saliency map that is derived by analyzing the features within an image, often using methods like semantic segmentation or by analyzing features such as color and contrast. In this research, after preliminary evaluation, the saliency feature map is adopted because of its superior performance compared to pure saliency and ICA saliency maps.

4.3.2.2. *Grad-CAM visualization*

Grad-CAM: In the AI context, a saliency map is a general term for a visualization highlighting important image regions, while Grad-CAM (Gradient-weighted Class Activation Mapping) is a specific, gradient-based technique for generating these maps in convolutional neural networks (CNNs) [74–76]. Grad-CAM combines feature map activations with gradient information to produce a heatmap showing which parts of an image led to a CNN's decision for a specific class, offering a more detailed and interpretable view than generic saliency maps.

Both Grad-CAM and occlusion sensitivity provide valuable but different perspectives on model decision-making. Grad-CAM offers efficiency and a view into the model's internal representations, while occlusion sensitivity provides a more direct and sometimes more precise measure of feature importance. Furthermore, Grad-CAM uses class-discriminative feature maps derived from the model's gradients to highlight important regions in an image; whereas local interpretable model-agnostic explanation (LIME) explains predictions by creating a local, interpretable, model-agnostic model by perturbing the input image [74–76]. Grad-CAM is a heatmap-based method specific to CNNs, while LIME is a model-agnostic technique that can be applied to any black-box model and is not limited to image analysis [74,76].

In this research, after preliminary evaluation of the visualization based on the three methods, the DenseNet-based Grad-CAM with the LIME algorithm has been adopted because of its unique visualization performance compared to pure Grad-CAM and occlusion sensitivity.

4.4. Implementation of the complete CNN algorithmic model based on DenseNet model structure for adaptive classification of chest diseases

4.4.1. *Implementation strategy*

The implementation of the CNN algorithm based on the DenseNet model structure is illustrated diagrammatically in Figure 19. After data pre-processing, the class label distributions on the data set are listed in Table 2. The size of the input images for different CNNs were different and therefore the datasets were pre-processed to resize the X-Ray images. In the classification problem for DenseNet, the images were resized to 320 × 320 pixels. All images were normalized using Z-score normalization based on the image database mean and standard deviation. The implementation of the CNN algorithm based on the DenseNet model structure is summarized as follows:

1. Input image is passed through a series of convolutional layers that extract features using convolutional filters with appropriate stride and padding techniques.
2. The output of each layer is passed through a rectified linear unit (ReLU) activation function to introduce non-linearity.
3. Pooling layers are used to reduce dimensionality of output and make the model more efficient.
4. The convolutional and pooling layers computations are repeated 5 times at each epoch due to the complexity of the chest X-ray classification problem.
5. The output of the final convolutional layer is flattened and fed into the fully connected layer (FC Layer) that performs classification on the extracted features from the chest X-ray images.
6. The output of the FC layer is passed through a softmax activation function with the associated cost functions to produce a class label for the input image.
7. The implementation of the CNN algorithm based on the DenseNet model structure for each chest disease classification converged after 80 epochs (iterations) which demonstrate the robustness of the algorithm (see Figure 20(a)).
8. As discussed in Section IV(C), the saliency feature maps and the corresponding DenseNet-based Grad-CAM with LIME algorithm for the 14 classes of chest diseases inherent in the CXR images discussed and shown in Figure 2 to Figure 16 are presented in Figure 21(a) and (b). The saliency feature maps shows the segments of the chest that are infected with the yellowish heatmap while the DenseNet-based Grad-CAM shows the specific patched segments that are infected for direct interpretation and diagnosis. It is evident from the DenseNet Grad-CAM with LIME results of Figure 21(a) and (b) that chest disease can be transmitted to and from other parts of the whole body.

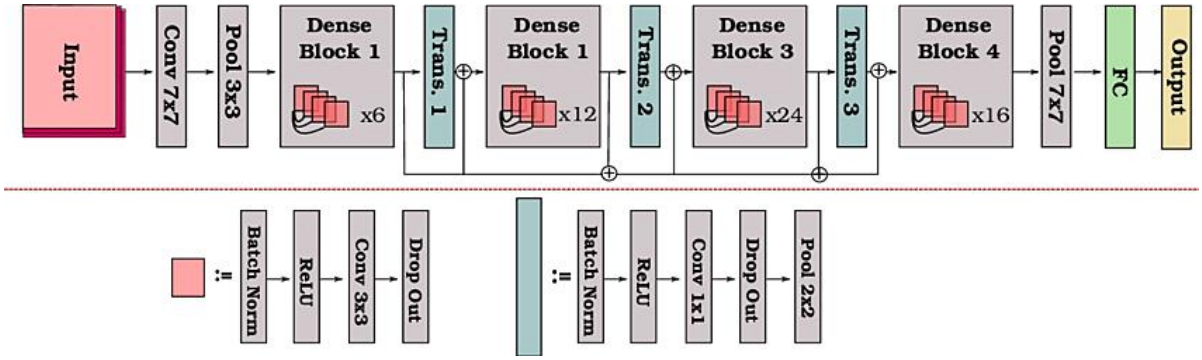

Figure 18. The CNN Algorithmic model based on DenseNet model structure

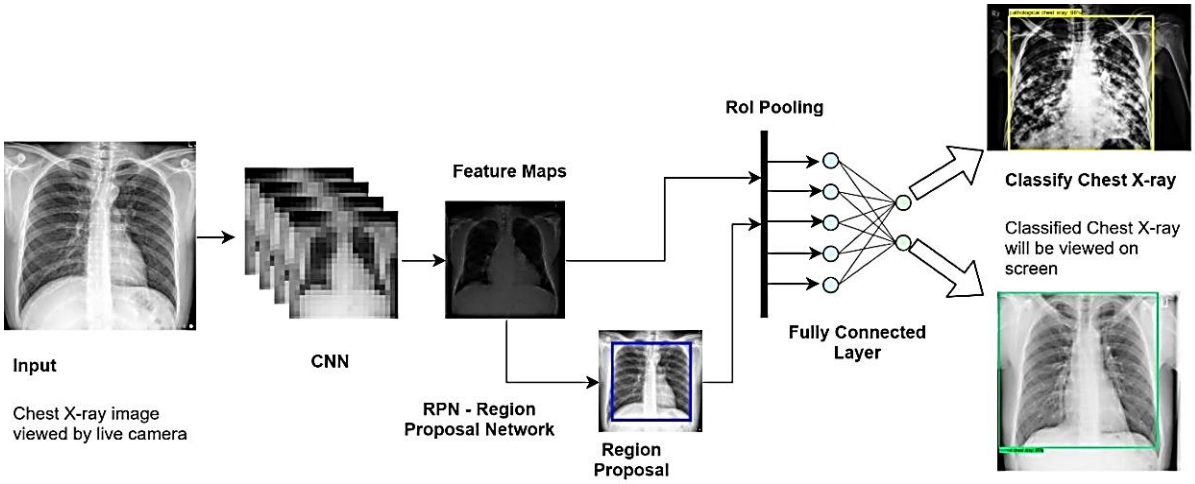

Figure 19. Implementation of the complete CNN Algorithmic model for adaptive classification of chest x-ray diseases based on DenseNet model

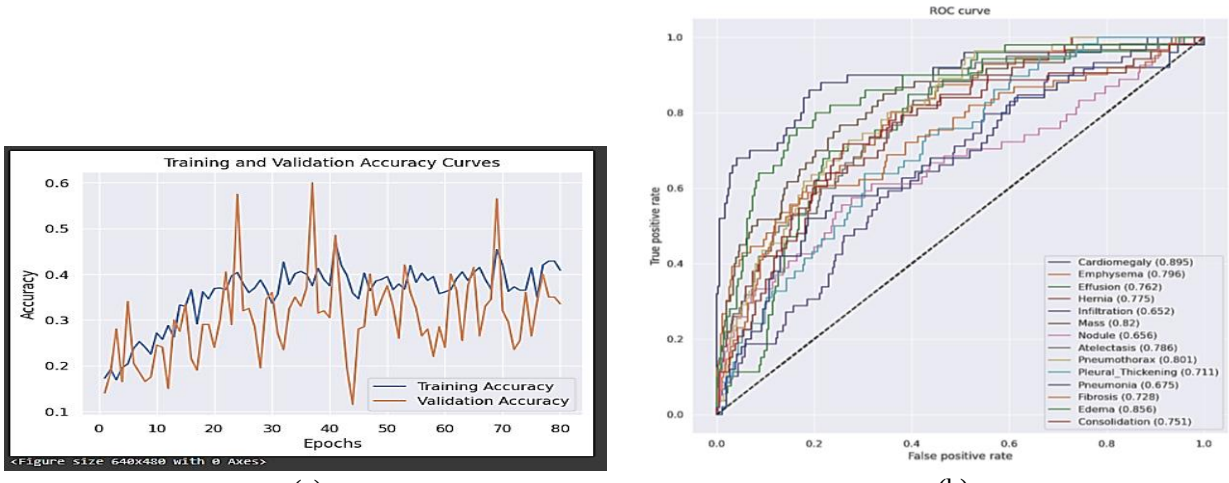

(a) (b)

Figure 20. Training and validation results for 80 iterations obtained by deep CNN based on DenseNet model structure: (a) Accuracy curves and (b) AUC-ROC curves and values for the 14 CXR disease of Figure 4 to Figure 17.

4.4.2. *Additional Implementation Considerations*

The methodology for developing and implementing the CNN based on DenseNet model algorithm for the accurate detection and classification of the 14 different chest diseases involves additional consideration listed as follows:

1. Data Preprocessing: Cleaned and preprocessed the dataset to ensure consistency and quality. This includes resizing the images, normalizing pixel intensities, and handling missing data although there was no missing data.

2. Data Split: For the chest pathology detection and classification task, the dataset were split into training and

validation while the test data set were acquired separately. The training data set was used to train the model, the validation set was used for hyperparameter tuning and model selection, and the testing set was used for unbiased evaluation of the final performance of the CNN based on DenseNet model structure.

3. Model Structure Selection: Choosing an appropriate deep learning model structure suitable for image classification tasks. DenseNet was used because it balances model complexity, computational efficiency, and performance.

4. Model Training: The training starts by loading the DenseNet121 model. DenseNet121 is a pre-trained deep learning structure known for its effectiveness in various computer vision tasks. The model by adding additional layers specifically a global average pooling layer, which reduces the spatial dimensions of the output and prepares the DenseNet model for classification and a softmax layer with a sigmoid activation function. The model is then compiled using the Adam optimizer and a custom loss function. The custom loss function, *get_weighted_loss*, incorporates class weights to address class imbalance in the dataset. These weights are learned from a large dataset and serve as a starting point for the fine-tuning

process. During training, the CNN based on DenseNet model learns to recognize patterns and features indicative of the presence or absence of each disease. The training parameters option is presented in Table 3 [11].

5. Hyperparameter Tuning: Fine-tuned the model's hyperparameters to improve its performance. This involved adjusting learning rates, regularization techniques, batch sizes, and the number of layers and filters in the DenseNet architecture. The detailed hyperparameters used for tuning the deep CNN models are listed in Table 3 [40, 77]. Hyperparameter tuning was typically performed using the validation set [11].

6. Model Evaluation: Assessed the trained model performance using the testing set, which was not seen by the model during training or hyperparameter tuning. Evaluated various performance metrics such as accuracy, precision, and area under the receiver operating characteristic curve (AUC-ROC) to measure the model's effectiveness in accurately detecting the 14 target diseases. The model assigns a probability score to each class (e.g., probability of being normal and probability of being abnormal).

7. Iterative Refinement: Iterated and refined the model based on the evaluation results and feedback. This involved revisiting the model architecture, adjusting hyperparameters, or incorporating additional data or techniques to address specific challenges or limitations identified during the evaluation.

8. Interpretability and Explainability: Developed techniques to interpret and explain the model's predictions. This include generating heatmaps to highlight regions of interest in the chest X-ray images and applying attention mechanisms to understand the model's decision-making process. Interpretable models are crucial for gaining insights and building trust in the medical domain [24].

9. Validation and Deployment: Validated the model's performance on external datasets to assess its generalizability.

5. CNN simulation results and discussions of results based on the densenet model

The model is designed for chest X-ray diagnosis, aiming to identify 14 different diseases using deep learning techniques. The architecture used is DenseNet121. DenseNet121 is a type of Convolutional Neural Network (CNN) pre-trained model structure that has demonstrated success in various computer vision tasks, including medical image analysis. Each layer receives input not just from the previous layer but from all preceding layers. This encourages feature reuse and enhances the flow of information through the network. This model has been trained on a large dataset of labeled chest X-rays, where each image is linked to the presence or absence of specific chest diseases.

The loss function used during training guides the model to minimize the difference between predicted and actual label distributions. The training process involves adjusting the model's parameters to minimize the difference between predicted and actual labels. For each chest X-ray image, the model generates predictions for the presence or absence of 14 diseases, assigning a probability to each class. The probabilities represent the model's confidence in its predictions. The final layer of the DenseNet121 model consists of 14 neurons, each corresponding to one of the diseases. A suitable activation function, softmax, was applied to convert the model's raw output into probabilities. The extracted features are fed into a trained classification model. Based on the extracted features and the internal logic of the model, probabilities are assigned to each disease, indicating the likelihood of its presence in the X-ray.

The results are presented as a list of diseases along with associated probabilities. Each probability represents the model's estimate of the likelihood of a specific disease being present. A threshold, often set by medical professionals, can be applied to convert probabilities into binary predictions (presence or absence of a disease). For example, if the threshold is 0.5, probabilities above 0.5 are considered positive predictions. The training and validation results for the accuracy and rate of convergence (ROC) curves are shown in Figure 20(a) and (b) respectively. For space economy, only simulation results for four case studies with absolute chest disease classification from CXR images based on probabilities have been presented with performance comparison metrics tables.

5.1. Case study 1: high risk of cardiac and respiratory heart attack

The performance metrics for the deep CNN based on DenseNet, InceptionV3 and ResNet model structures for CASE STUDY 1 is shown in Table 4 where three CNN model structures have been tested in terms of

performance comparison for the chest disease classification based on CXR images.

The results are analyzed to assess the performance of three model structures using multiple metrics discussed in Section IV(B)(b) which include (i) Binary Accuracy, (ii) Precision, (iii) Recall, (iv) F1-score, (v) area under receiver operating characteristic curve (AUC-ROC), and (vi) Confusion Matrix.

Accuracy is an important metric in deep learning that shows the proportion of correctly predicted samples over the total number of samples according to (13). As it can be seen in the second row of Table 4, the DenseNet has the best accuracy of 99.29% when compared to InceptionV3 and ResNet models with accuracy of 71.43% and 68.72% respectively.

Precision is another important metric which shows the proportion of correct identifications. In terms of precision, the DenseNet outperforms the InceptionV3 and ResNet model structures as evident in the third row of Table 4. The DenseNet has a 99.15% precision when compared to the averagely 71.35% and 68.64% recorded by the Inception and ResNet models.

The recall score measures how well the model correctly captures positive cases. It is the ratio of the true positives to the sum of the true positives and false negatives. In this study, the proposed CNN based on the DenseNet model structure achieved an outstanding recall rate of 99.64% when compared to the 71.70% and 68.98 obtained using the InceptionV3 and ResNet models respectively. This extremely high recall rates emphasize the effectiveness of the DenseNet model in identifying positive cases correctly, hence reducing false negatives.

F1-score represents the harmonic mean of precision and recall. In terms of the F1-score, the deep CNN based on the DenseNet model structure shows superior performance than the InceptionV3 and the ResNet model structures with an F1-score of 99.52% signifying a balanced performance in precision and recall.

The Area Under the Receiver Operating Characteristic Curve (AUC-ROC) evaluates the performance of a model across all possible classification threshold, balancing sensitivity and specificity. In this study, the CNN based on DenseNet model structure achieved the highest AUC-ROC score across all slices, boasting a near-perfect score of 99.37%.

The confusion matrices for the deep CNN based on the proposed DenseNet, InconceptionV3 and ResNet model structures are shown respectively in Figure 22(a), (b) and (c) for Case study 1. It is obvious in Figure 22(a) the accuracy of 99.29% obtained by the DenseNet model justifies the robust performance the DenseNet model when compared to the InceptionV3 and ResNet models. The accuracy obtained from the confusion matrix construction is unarguably exactly the same as that shown in Table 4 for the three models. Thus, the confusion matrix shows that the DenseNet model performs well in accurately detecting both TP, TN, FP and FN for the predicted classified and class target outputs as shown in Figure 22.

Other results obtained for Case Study 1 based on probability scores for different chest X-ray diagnoses predicted by the deep learning model shown in Figure 23 are listed in Table 5 for high risk of cardiac and respiratory heart attack. Each label corresponds to a specific disease, and the associated score represents the confidence or probability of the model predicting that particular disease.

1. Cardiomegaly (0.82): The model predicts Cardiomegaly with a high confidence score, indicating an increased size of the heart. This condition may be associated with various cardiac issues.

2. Emphysema (0.70): The model predicts Emphysema with a substantial confidence score, suggesting potential damage to the air sacs in the lungs. This could be indicative of a chronic obstructive pulmonary disease (COPD).

Table 2. Class label distribution on data set

S/N	Labels	Distributions
1	No finding	60,361
2	Cardiomegaly	2776
3	Infiltration	19894
4	Emphysema	2516
5	Effusion	13317
6	Atelectasis	11559
7	Nodule	6331
8	Mass	5782
9	Consolidation	4667
10	Pneumothorax	5302
11	Pleural thickening	3385
12	Edema	2303
13	Fibrosis	1686
14	Pneumonia	1431
15	Hemia	227
Total label distribution		141,537

Table 3. Hyperparameter Training and Tuning options

S/N	Parameter and Layer Type	Specification
1	imageInputLayer	[32 32 1]
2	Convolution2dLayer	(5, 20)
3	reluLayer	empty
4	maxPooling2dLayer	2
5	Stride	2
6	Dropout Rates	0.5
7	L2Regularization	[1e-8 1e-2]
8	Momentum	[0.5 0.99]
9	Sequence padding Direction	Left
10	Padding	2
11	fullyConnectedLayer	14
12	Hyperparameter Optimizer	Adam
13	Loss Function	Cross entropy
12	MaxEpochs	100
13	Initial Learning Rate	[1e-3 1]
14	Gradient Algorithm Threshold	1
15	Shuffle	Every epoch
16	Metrics	accuracy

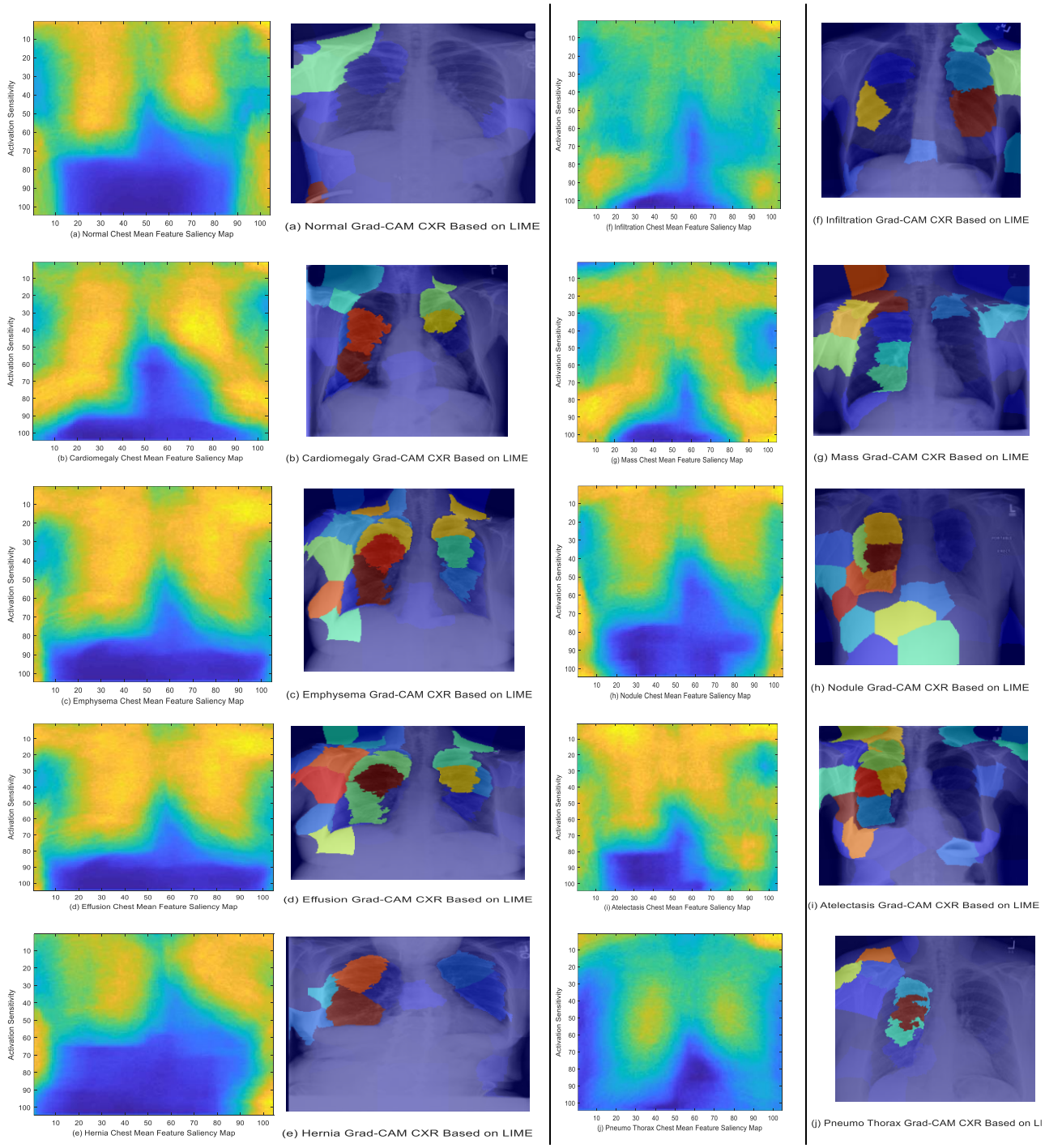

Figure 21. (a). Visualization comparison of the saliency map and the DenseNet-based Grad-CAM with LIME for CXR

Table 4. Performance comparison metrics for the deep CNN based on DenseNet, InceptionV3 and ResNet model structures for Case Study 1

S/N	Performance Metrics	CNN Pre-trained Model Structures		
		DenseNet	InceptionV3	ResNet-50
1	Accuracy	99.29	71.43	68.72
2	Precision	99.15	71.35	68.64
3	Recall	99.64	71.70	68.98
4	F1-Score	99.52	71.62	68.90
5	AUC-ROC	99.37	71.51	68.80

10.57647/ijbbe.2025.0502.09

3. Effusion (0.29): The model predicts Effusion with a lower confidence score, implying the possible presence of excess fluid around the lungs. Further investigation may be needed.

4. Hernia (0.83): The model predicts Hernia with high confidence, indicating a protrusion of an organ through the abdominal wall. This requires clinical attention.

5. Infiltration (0.34): The model predicts Infiltration with moderate confidence, suggesting the presence of substances such as fluid or inflammation in the lung tissues.

6. Mass (0.26): The model predicts Mass with a relatively low confidence score. While it may indicate a mass or tumor, further evaluation is needed.

7. Nodule (0.36): The model predicts Nodule with moderate confidence, pointing to the possibility of small, rounded abnormalities in the lung.

8. Atelectasis (0.18): The model predicts Atelectasis with a low confidence score, suggesting partial lung collapse. Clinical assessment is essential.

9. Pneumothorax (0.19): The model predicts Pneumothorax with low confidence, indicating potential air leakage into the pleural space. Further investigation is required.

10. Pleural Thickening (0.71): The model predicts Pleural Thickening with high confidence, suggesting thickening of the membrane around the lungs. This may be associated with various conditions.

11. Pneumonia (0.19): The model predicts Pneumonia with low confidence, implying a lower probability of infection in the lungs.

12. Fibrosis (0.80): The model predicts Fibrosis with high confidence, indicating scarring of lung tissue. This may be associated with various lung diseases.

13. Edema (0.08): The model predicts Edema with a low confidence score, suggesting a potential accumulation of fluid. Clinical assessment is crucial.

14. Consolidation (0.11): Interpretation: The model predicts Consolidation with a low confidence score, indicating a region of the lung filled with liquid. Further investigation is necessary.

5.1.1. *risk of heart disease for cardiac and respiratory heart attack predictions for case 1*

Based on the predictions, there are indications that the patient may be at risk of certain cardiac and respiratory conditions. Specifically, the high predictions for Cardiomegaly, Hernia, and Pleural Thickening warrant attention and further evaluation by healthcare professionals. It is important to note that the model's predictions are probabilities, and a comprehensive diagnosis should involve a medical expert's assessment, possibly including additional tests and patient history.

5.1.2. *Overall Interpretation for CASE 1*

The model highlights potential concerns for cardiomegaly, emphysema, hernia, pleural thickening, and fibrosis, with high confidence in the first three as shown in Table 6.

Table 5. Probabilities for high risk of cardiac and respiratory heart attack for Case Study 1

S/N	Classes	Probability
1	Cardiomegaly	0.82
2	Emphysema	0.70
3	Effusion	0.29
4	Hernia	0.83
5	Infiltration	0.34
6	Mass	0.26
7	Nodule	0.36
8	Atelectasis	0.18
9	Pneumothorax	0.19
10	Pleural Thickening	0.71
11	Pneumonia	0.19
12	Fibrosis	0.80
13	Edema	0.08
14	Consolidation	0.11

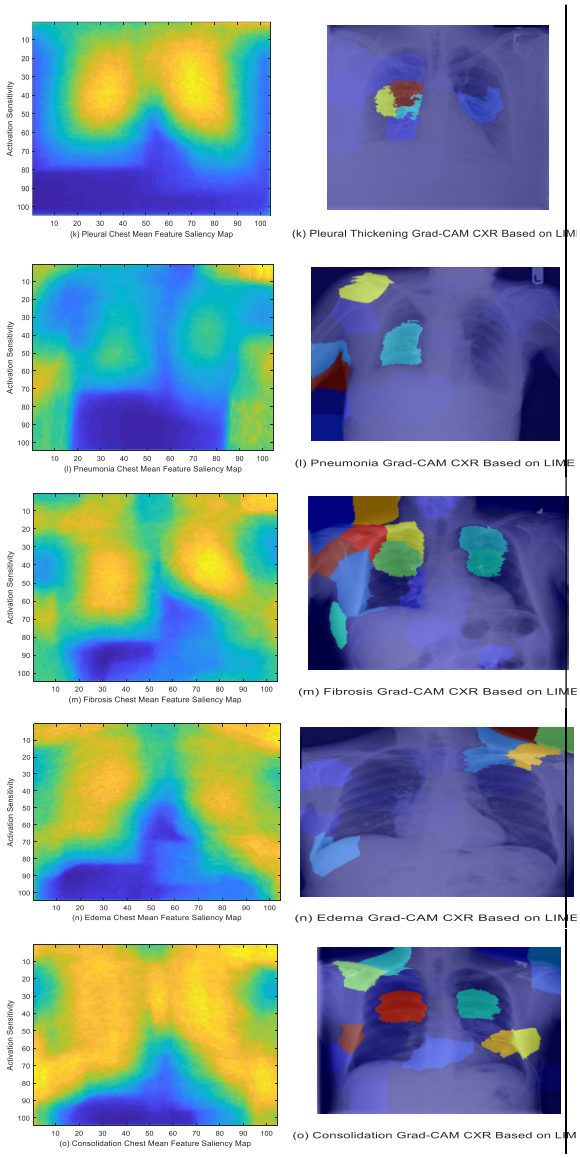

Figure 21. (b) Visualization comparison of the saliency map and the DenseNet-based Grad-CAM with LIME for CXR

Table 6. Confidence predictions for cardiac and respiratory heart attack probabilities for Case Study 1

High Confidence Predictions	Cardiomegaly (0.82), Emphysema (0.70), Hernia (0.83), Pleural Thickening (0.71), Fibrosis (0.80)
Low Confidence Predictions	Effusion (0.29), Infiltration (0.34), Mass (0.26), Nodule (0.36), Atelectasis (0.18), Pneumothorax (0.19), Pneumonia (0.19), Edema (0.08), Consolidation (0.11)

Table 7. Performance comparison metrics for the deep CNN based on DenseNet, InceptionV3 and ResNet model structures for Case Study 2

S/N	Performance Metrics	CNN Pre-trained Model Structures		
		DenseNet	InceptionV3	ResNet-50
1	Accuracy	99.89	74.21	72.27
2	Precision	99.72	74.08	72.15
3	Recall	99.88	74.20	72.26
4	F1-Score	99.69	74.06	72.12
5	AUC-ROC	99.86	74.19	72.25

Table 8. Predicted probabilities for low likelihood of heart enlargement for Case Study 2

S/N	Classes	Probability
1	Cardiomegaly	0.06
2	Emphysema	0.47
3	Effusion	0.88
4	Hernia	0.56
5	Infiltration	0.55
6	Mass	0.75
7	Nodule	0.51
8	Atelectasis	0.32
9	Pneumothorax	0.85
10	Pleural Thickening	0.96
11	Pneumonia	0.46
12	Fibrosis	0.82
13	Edema	0.21
14	Consolidation	0.61

Table 9. Confidence predictions for low likelihood heart enlargement for Case Study 2

High Confidence Predictions	Pleural Thickening (0.96), Pneumothorax (0.85), Fibrosis (0.82), Mass (0.75), Effusion (0.88).
Low Confidence Predictions	Cardiomegaly (0.06), Atelectasis (0.32), Nodule (0.51), Edema (0.21), Pneumonia (0.46).

It suggests further investigation for effusion and infiltration, but their likelihoods are relatively low. Other diseases like mass, nodule, atelectasis, pneumothorax, pneumonia, edema, and consolidation are unlikely based on the model's predictions.

5.2. Case study 2: low likelihood of heart enlargement

The performance comparison metrics of the deep CNN based on DenseNet, InceptionV3 and ResNet model structures are summarized in Table 7. Due to space economy, the confusion matrix is not shown. As discussed in Case Study 1, the simulation results for Case Study 2 are analyzed to assess the performance of three model structures using the following metrics: (i) Binary Accuracy, (ii) Precision, (iii) Recall, (iv) F1 score, (v) area under receiver operating characteristic curve (AUC-ROC), and (vi) Confusion Matrix. It is evident that the CNN based on the DenseNet model structure outperforms the InceptionV3 and ResNet models.

Furthermore, the simulation results obtained for Case Study 2 based on probability scores for different chest X-ray diagnoses predicted by the deep learning model shown in Figure 24 are listed in Table 8 for low likelihood of heart enlargement. Each label corresponds to a specific disease, and the associated score represents the confidence or probability of the model predicting that particular disease.

1. Cardiomegaly (0.06): The model predicts a low probability of Cardiomegaly. While this result suggests a lower likelihood of an enlarged heart, it's crucial to consider clinical symptoms and other diagnostic information.

2. Emphysema (0.47): The model predicts a moderate probability of Emphysema, indicating potential damage to air sacs. This may be associated with chronic lung conditions.

3. Effusion (0.88): The high probability of Effusion suggests a high likelihood of fluid accumulation around the lungs. This may require immediate medical attention.

4. Hernia (0.56): The model predicts a moderate probability of Hernia. This could indicate a protrusion of an organ through the abdominal wall, requiring further clinical examination

5. Infiltration (0.55): The moderate probability of Infiltration implies potential substances, such as fluid or inflammation, in lung tissues. Clinical evaluation is recommended.

6. Mass (0.75): The model predicts a high probability of a Mass, suggesting the presence of a tumor or abnormal growth. Immediate medical attention is advised.

7. Nodule (0.51): The moderate probability of a Nodule indicates the possibility of small, rounded abnormalities in the lung. Further diagnostic tests may be needed.

8. Atelectasis (0.32): The model predicts a moderate probability of Atelectasis, suggesting partial lung collapse. Clinical assessment is important for a comprehensive diagnosis.

9) Pneumothorax (0.85): The high probability of Pneumothorax indicates a strong likelihood of air leakage into the pleural space. This is a serious condition that requires immediate medical attention.

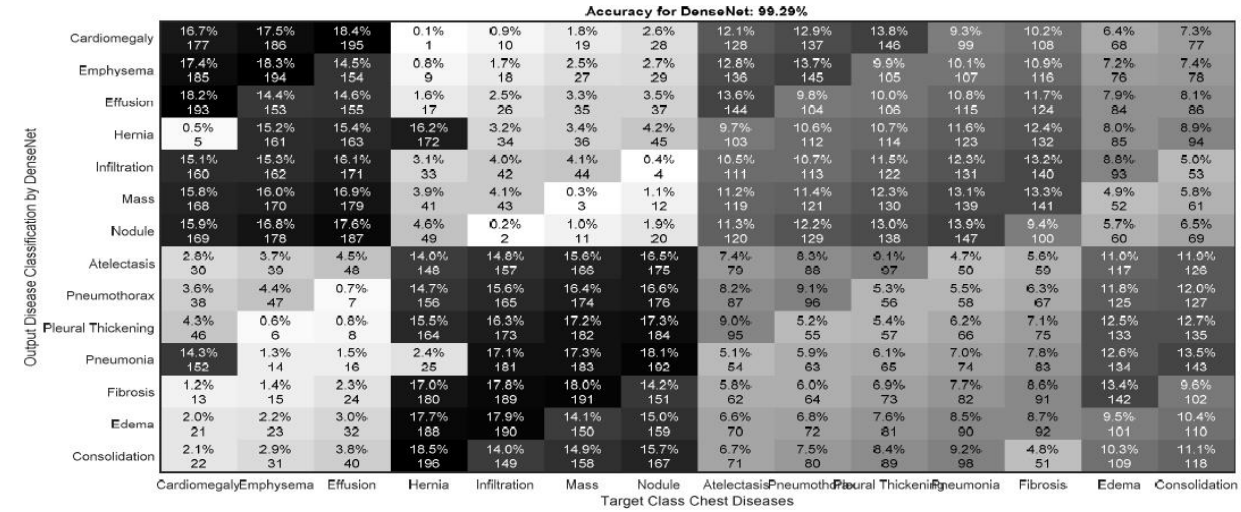

(a)

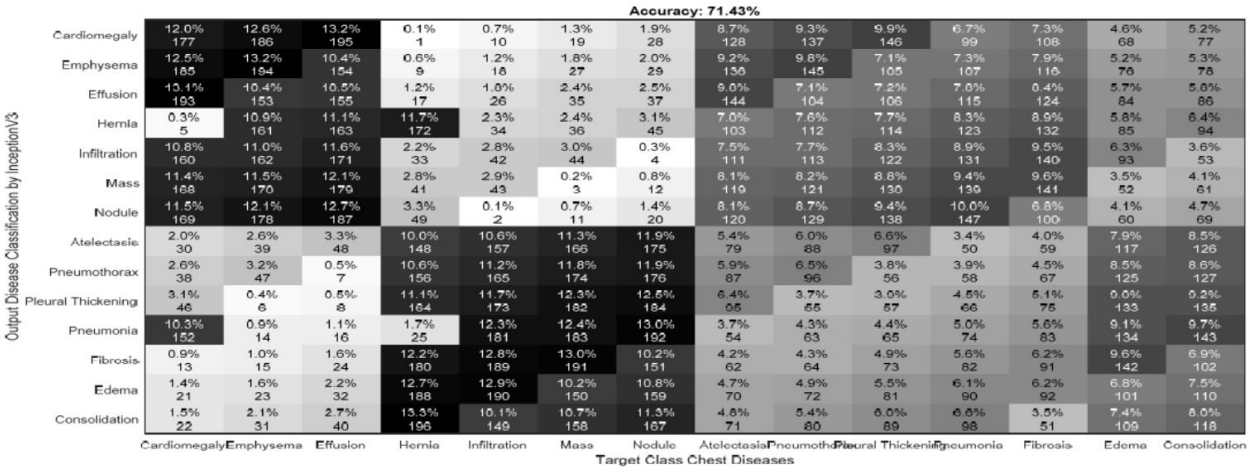

(b)

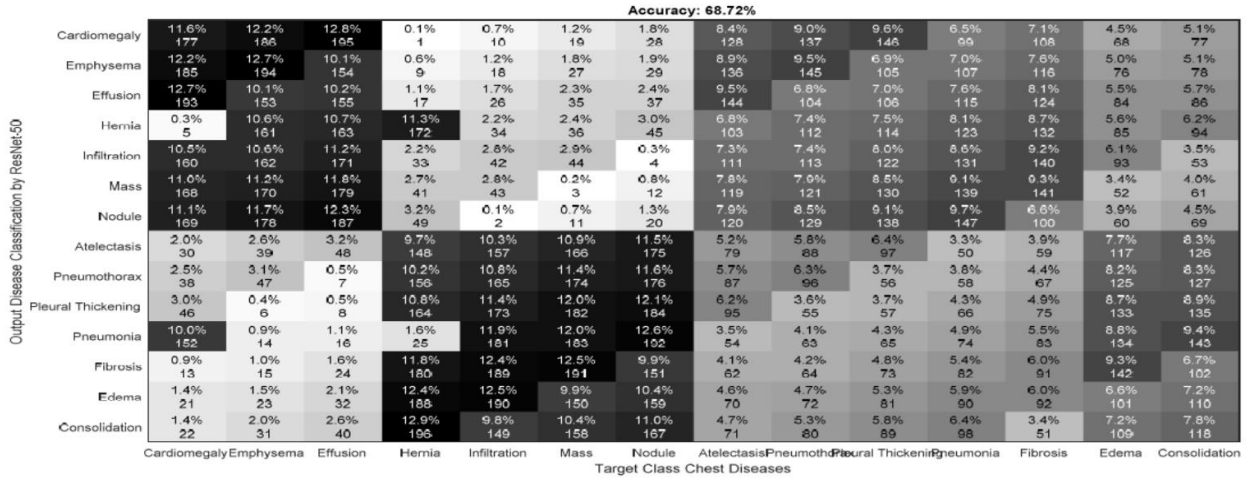

(c)

Figure 22. Confusion matrix with class accuracy for the deep CNN with different model structures for Case Study 1: (a) DenseNet, (b) InceptionV3, and (c) ResNet-50

10.57647/ijbbe.2025.0502.09

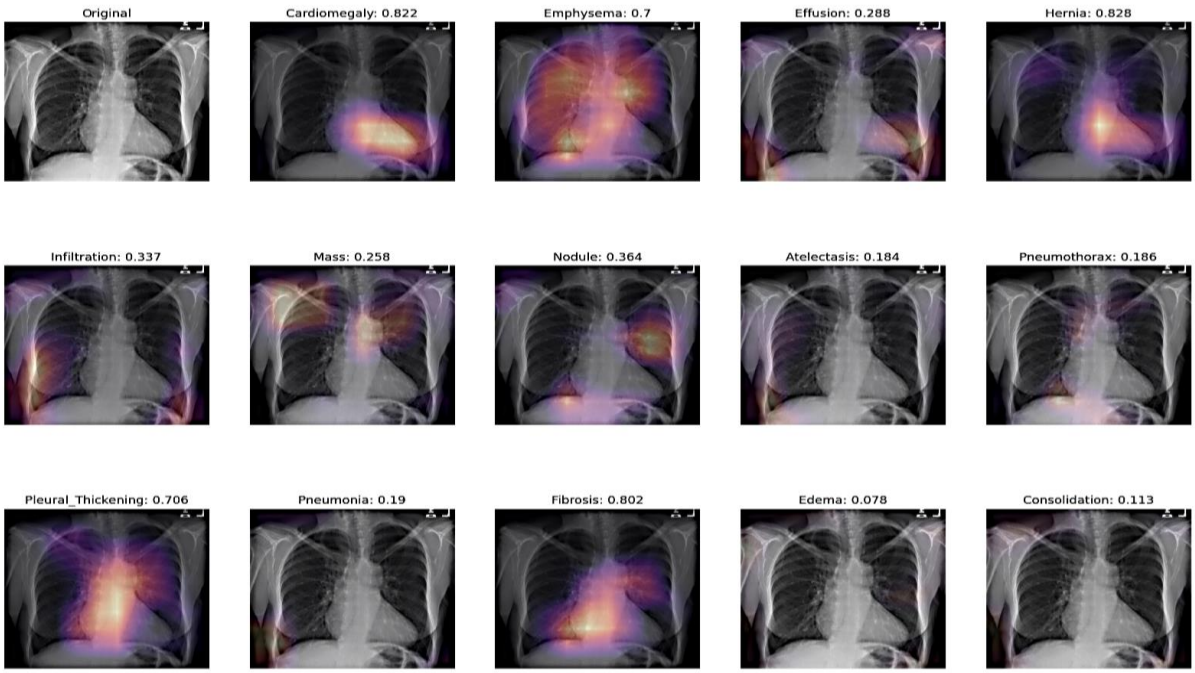

Figure 23. Chest X-ray classification results for high risk of cardiac and respiratory heart attack for Case Study 1

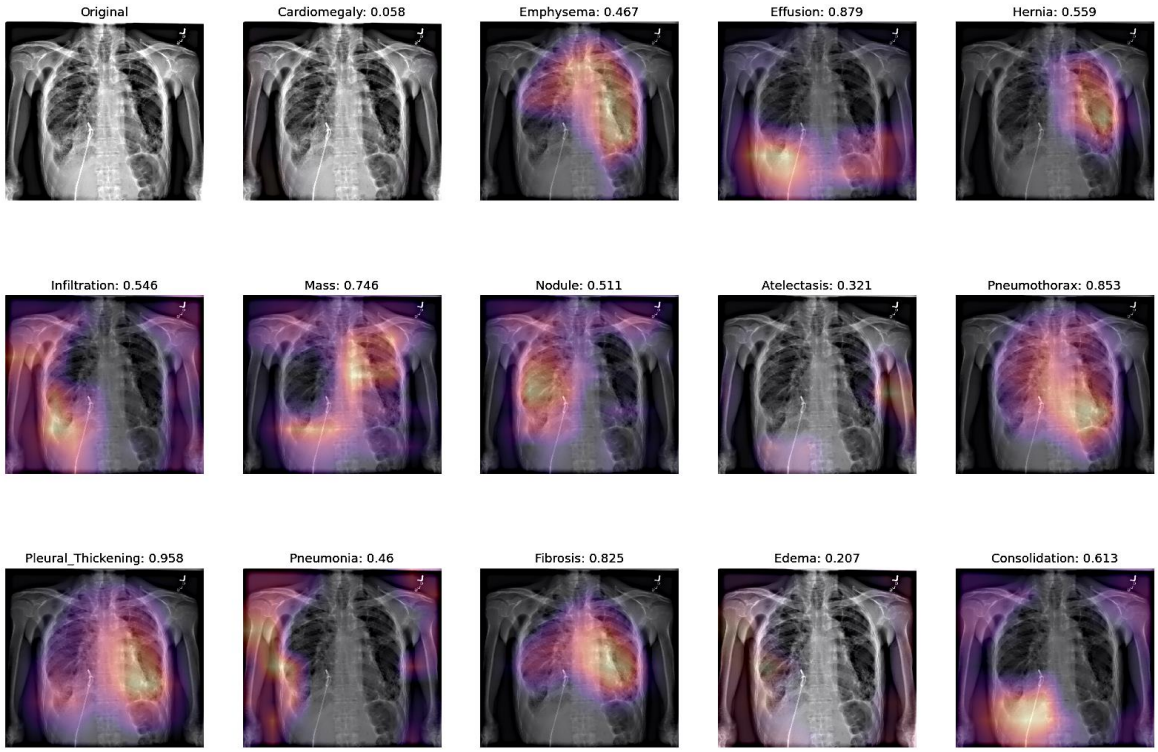

Figure 24. Chest X-ray classification results for low likelihood heart enlargement for Case Study 2

10. Pleural Thickening (0.96): The very high probability of Pleural Thickening suggests a significant thickening of the membrane around the lungs. This may be indicative of various respiratory conditions.

11. Pneumonia (0.46): The moderate probability of Pneumonia implies a likelihood of lung infection. Clinical evaluation and additional tests are needed for confirmation.

12. Fibrosis (0.82): The model predicts a high probability of Fibrosis, indicating scarring of lung tissue. This may be associated with chronic lung diseases.

13. Edema (0.21): The low probability of Edema suggests a lower likelihood of fluid accumulation. Clinical correlation is essential for a comprehensive diagnosis.

14. Consolidation (0.61): The moderate probability of

10.57647/ijbbe.2025.0502.09

Consolidation indicates a region of the lung filled with liquid. Further diagnostic tests and clinical evaluation are recommended.

5.2.1. *Risk of heart disease for low likelihood heart enlargement for case 2*

Considering the low probability assigned to Cardiomegaly (0.06) as shown in Table 9, the patient appears to have a lower likelihood of an enlarged heart based on the model's prediction.

5.2.2. *Overall interpretation for case 2*

The model highlights potential concerns for pleural thickening, pneumothorax, fibrosis, mass, and effusion, with very high confidence in the first two. It suggests further investigation for emphysema, hernia, infiltration, and consolidation. Other diseases like cardiomegaly, atelectasis, edema, and pneumonia are less likely based on the model's predictions.

5.3. Case study 3: lower risk of cardiac-related disease

The performance comparison metrics of the deep CNN based on DenseNet, InceptionV3 and ResNet model structures are shown in Table 10. Again, due to space economy, the confusion matrix for Case Study 3 is not shown. As can be seen in Table 10, the performance comparison metrics show that the deep CNN based on the DenseNet model structure has the best and highest predicted classification results with: (i) Binary Accuracy of 99.94%, (ii) Precision of 99.89%, (iii) Recall value of 99.77%, (iv) F1-score of 99.81%, and (v) area under receiver operating characteristic curve (AUC-ROC) value of 99.90%. It is evident from Table 10 that the CNN based on the DenseNet model structure outperforms the InceptionV3 and ResNet models.

Other simulation results obtained for third case study based on the probability scores for different chest X-ray diagnoses predicted by the deep learning model for lower risk of cardiac-related diseases shown in Figure 25 with the corresponding probabilities listed in Table 11. Each label corresponds to a specific disease, and the associated score represents the confidence or probability of the model predicting that particular disease.

1. Cardiomegaly (0.09): The model predicts a low probability of Cardiomegaly, indicating a relatively lower chance of an enlarged heart. Further clinical evaluation is needed for confirmation.
2. Emphysema (0.04): The model predicts a low probability of Emphysema, suggesting a lower likelihood of damage to air sacs. However, clinical correlation is crucial for accurate diagnosis.
3. Effusion (0.03): The low probability of Effusion implies a lower chance of fluid accumulation around the lungs. This may be a positive indicator, but clinical assessment is necessary.
4. Hernia (0.06): The model predicts a moderate probability of Hernia. This could indicate a protrusion of an organ through the abdominal wall, warranting further clinical examination.
5. Infiltration (0.28): The moderate probability of Infiltration suggests potential substances, such as fluid or inflammation, in lung tissues. Clinical evaluation and additional tests are recommended.
6. Mass (0.06): The model predicts a low probability of a Mass, indicating a lower likelihood of a tumor or abnormal growth. Clinical correlation is essential for a comprehensive diagnosis.
7. Nodule (0.09): The model predicts a low to moderate probability of a Nodule, suggesting the possibility of small, rounded abnormalities in the lung. Further diagnostic tests may be needed.
8. Atelectasis (0.06): Interpretation: The model predicts a low probability of Atelectasis, indicating a lower likelihood of partial lung collapse. Clinical assessment is important for a comprehensive diagnosis.
9. Pneumothorax (0.06): The low probability of Pneumothorax suggests a lower likelihood of air leakage into the pleural space. This is a positive indicator, but clinical assessment is necessary.
10. Pleural Thickening (0.05): The low probability of Pleural Thickening suggests a lower chance of significant thickening of the membrane around the lungs. Clinical correlation is essential for confirmation.
11. Pneumonia (0.09): The model predicts a low probability of Pneumonia, indicating a lower likelihood of lung infection. Clinical evaluation and additional tests are needed for confirmation.

Table 10. Performance comparison metrics for the deep CNN based on DenseNet, InceptionV3 and ResNet model structures for Case Study 3

S/N	Performance Metrics	CNN Pre-trained Model Structures		
		DenseNet	InceptionV3	ResNet-50
1	Accuracy	99.94	75.67	73.43
2	Precision	99.89	75.63	73.39
3	Recall	99.77	75.54	73.31
4	F1-Score	99.81	75.57	73.33
5	AUC-ROC	99.90	75.64	73.40

Table 11. Predicted probabilities for lower risk of cardiac-related disease for CASE 3

S/N	Classes	Probability
1	Cardiomegaly	0.09
2	Emphysema	0.04
3	Effusion	0.03
4	Hernia	0.06
5	Infiltration	0.28
6	Mass	0.06
7	Nodule	0.09
8	Atelectasis	0.06
9	Pneumothorax	0.06
10	Pleural Thickening	0.05
11	Pneumonia	0.09
12	Fibrosis	0.03
13	Edema	0.06
14	Consolidation	0.10

12. Fibrosis (0.03): The low probability of Fibrosis suggests a lower chance of scarring of lung tissue. Clinical correlation is crucial for an accurate diagnosis.
13. Edema (0.06): The model predicts a low probability of Edema, suggesting a lower likelihood of fluid accumulation. Clinical correlation is essential for confirmation.
14. Consolidation (0.10): The model predicts a moderate probability of Consolidation, indicating a region of the lung filled with liquid. Further diagnostic tests and clinical evaluation are recommended.

5.3.1. Risk of heart disease for case 3

Considering the low probability assigned to Cardiomegaly and the relatively lower probabilities of other cardiac-related conditions, the patient appears to have a lower overall risk of heart disease based on the model's prediction.

5.3.2. Overall interpretation for case 3

The model highlights Infiltration with 28% probability. This suggests the presence of abnormal tissue replacing healthy lung tissue. Other potentially significant findings are Consolidation, Cardiomegaly Nodule, Pneumonia, Hernia, Mass, Atelectasis, Edema, Pleural thickening, Emphysema, Effusion and Fibrosis.

5.4. Case study 4: potentially life-threatening cardiac conditions

The performance of chest diseases classification by the three deep CNN model structures, namely: DenseNet, InceptionV3 and ResNet are summarized in Table 12 where it is evident that the DenseNet model demonstrates high classification capabilities with the hightest scores in all the standard metrics considered. Again, due to space economy, the confusion matrix for Case Study 4 is not shown. As can be seen in Table 10, the DenseNet model structure has the best and highest predicted classification results with: (i) Binary Accuracy of 99.92%, (ii) Precision of 99.84%, (iii) Recall value of 99.81%, (iv) F1-score of 99.87%, and (v) area under receiver operating characteristic curve (AUC-ROC) value of 99.94%.

Other simulation results obtained for chest X-ray classification of case study 4 are shown in Figure 26 with the predicted probability scores for different chest X-ray diagnoses predicted by the deep learning model shown in Table 13. Each label corresponds to a specific disease, and the associated score represents the confidence or probability of the model predicting that particular disease.

1. Cardiomegaly (0.11): The model predicts a low probability of Cardiomegaly, suggesting a lower likelihood of an enlarged heart. Clinical correlation is needed for confirmation, especially if the patient exhibits relevant symptoms.
2. Emphysema (0.93): A high probability of Emphysema indicates a significant likelihood of damage to the air sacs in the lungs. This result raises concerns about potential respiratory issues, and further clinical evaluation is crucial.
3. Effusion (0.29): The model predicts a moderate probability of Effusion, suggesting a notable chance of fluid accumulation around the lungs. Clinical correlation and additional diagnostic tests are recommended.
4. Hernia (0.16): A low probability of Hernia suggests a lower likelihood of a protrusion of an organ through the abdominal wall. Further clinical examination is needed to confirm the absence of a hernia.
5. Infiltration (0.42): The moderate probability of Infiltration suggests potential substances, such as fluid or inflammation, in lung tissues. Clinical evaluation and additional tests are recommended for confirmation.
6. Mass (0.80): A high probability of Mass indicates a significant likelihood of a tumor or abnormal growth.
7. Nodule (0.57): The moderate to high probability of a Nodule suggests the possibility of small, rounded abnormalities in the lung. Further diagnostic tests, such as CT scans, may be needed for confirmation.
8. Atelectasis (0.49): The moderate probability of Atelectasis indicates a notable likelihood of partial lung collapse. Clinical correlation, imaging studies, and possibly bronchoscopy are crucial for accurate diagnosis and treatment.
9. Pneumothorax (0.91): The high probability of Pneumothorax suggests a significant likelihood of air leakage into the pleural space. Urgent clinical evaluation and imaging studies are necessary for prompt intervention.
10. Pleural Thickening (0.46): The moderate probability of Pleural Thickening suggests a notable chance of significant thickening of the membrane around the lungs. Clinical correlation and imaging studies are essential for confirmation.
11. Pneumonia (0.23): The model predicts a low to moderate probability of Pneumonia, indicating a likelihood of lung infection. Clinical evaluation and additional tests are needed for confirmation.
12. Fibrosis (0.08): A low probability of Fibrosis suggests a lower likelihood of scarring of lung tissue. Clinical correlation is crucial for an accurate diagnosis.
13. Edema (0.38): The moderate probability of Edema indicates a notable likelihood of fluid accumulation. Clinical correlation and additional tests are essential for confirmation.
14. Consolidation (0.49): The moderate probability of Consolidation indicates a notable chance of a region of the lung filled with liquid. Further diagnostic tests and clinical evaluation are recommended.
Urgent clinical correlation, imaging studies, and possibly a biopsy are essential for accurate diagnosis and treatment planning.

5.4.1. *Risk of heart disease for case 4*

Considering the collective probabilities and the relatively high probability of Emphysema, Mass, and Pneumothorax as shown in Table 14, there might be an increased risk of heart-related issues.

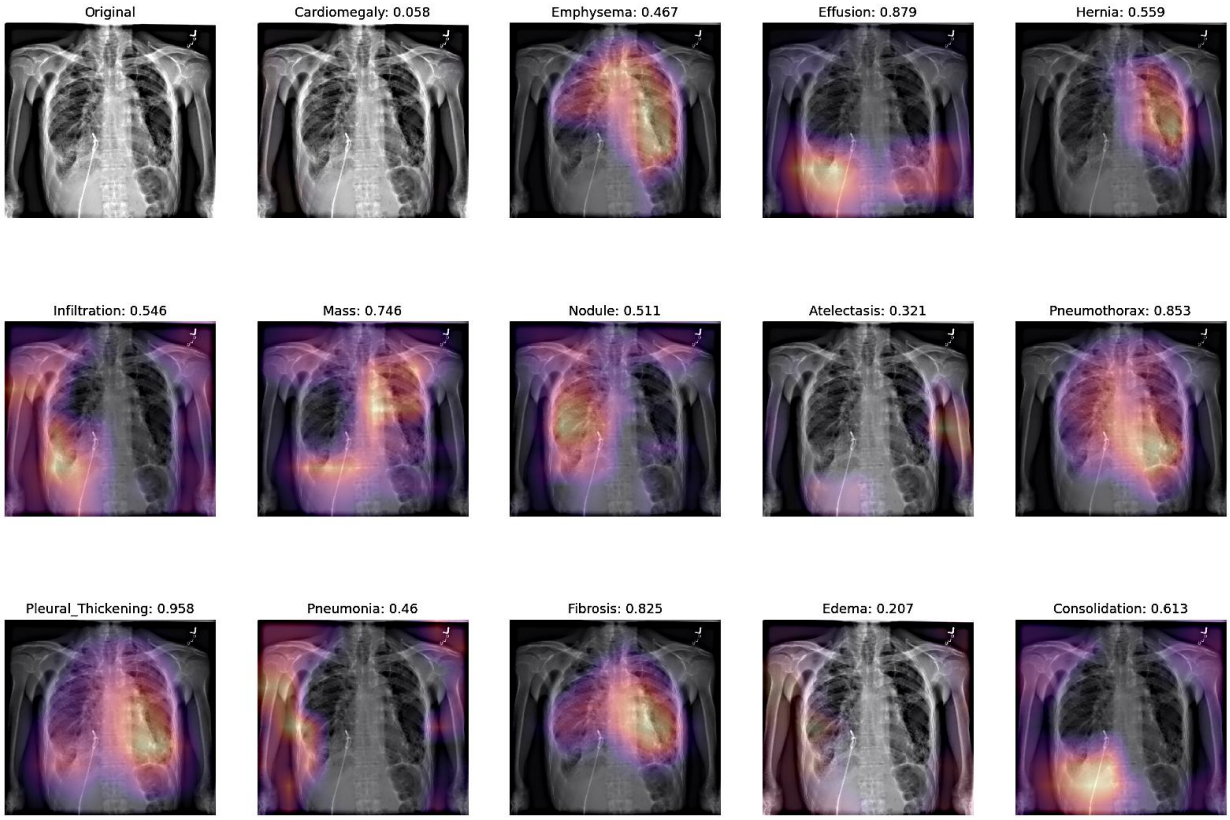

Figure 25. Chest X-ray classification results for low likelihood heart enlargement for Case Study 3

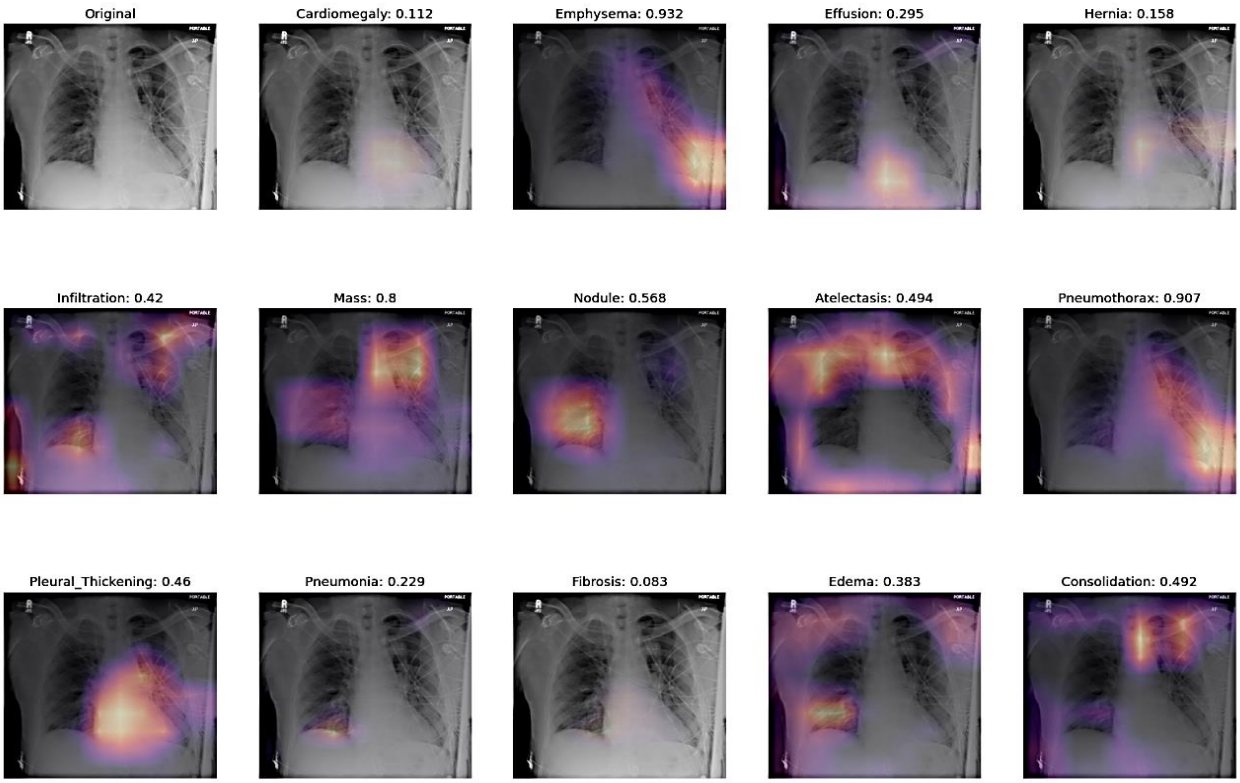

Figure 26. Chest X-ray classification results for potentially life-threatening cardiac conditions for Case Study 4

5.4.2. *Overall interpretation for case 4*

The model highlights Emphysema with 93% probability. This is the most likely finding, suggesting significant destruction of air sacs in the lungs, leading to breathing difficulties. This is a serious condition and requires prompt medical attention.

5.5. Deductions from the CNN simulation results based on the densenet model structure

The model's predictions are supportive but not definitive. The model requires correlation with clinical information, patient history, and potentially other diagnostic tests. The model serves as a valuable aid in the diagnostic process, providing a rapid screening tool to prioritize cases. The predicted probabilities of the chest X-ray classification results obtained in Section V(A) to Section V(D) are summarized in Table 15.

As it is evident in Table 15, the prediction probabilities assigned to each disease class, such as Cardiomegaly, Effusion, and Pneumothorax, provide a quantitative measure of the model's confidence in its predictions. The varying probabilities across classes suggest that the model exhibits an understanding of different diseases, capturing complex patterns in the chest X-ray images. For case 1, Cardiomegaly is predicted with high confidence, indicating an enlarged heart, possibly associated with cardiac issues.

Table 12. Performance comparison metrics for the deep CNN based on DenseNet, InceptionV3 and ResNet model structures for Case Study 4

S/N	Performance Metrics	CNN Pre-trained Model Structures		
		DenseNet	InceptionV3	ResNet-50
1	Accuracy	99.92	75.32	72.68
2	Precision	99.84	75.26	72.62
3	Recall	99.81	75.24	72.60
4	F1-Score	99.87	75.28	72.64
5	AUC-ROC	99.94	75.34	72.70

Table 13. Predicted probabilities for potentially life-threatening cardiac conditions for CASE 4

S/N	Classes	Probability
1	Cardiomegaly	0.11
2	Emphysema	0.93
3	Effusion	0.29
4	Hernia	0.16
5	Infiltration	0.42
6	Mass	0.80
7	Nodule	0.57
8	Atelectasis	0.49
9	Pneumothorax	0.91
10	Pleural Thickening	0.46
11	Pneumonia	0.23
12	Fibrosis	0.08
13	Edema	0.38
14	Consolidation	0.49

Table 14. Confidence predictions for potentially life-threatening cardiac conditions for Case Study 4

High Confidence Predictions	Emphysema (0.93), Pneumothorax (0.91), Mass (0.80).
Other Potentially Significant Findings	Infiltration (0.42), Nodule (0.57), Atelectasis (0.49), Pleural Thickening (0.46), Consolidation (0.49)
Low Confidence Predictions	Cardiomegaly (0.11), Effusion (0.29).

Table 15. Predicted Probabilities for the 4 different case studies

S/N	Classes	Probabilities			
		CASE 1	CASE 2	CASE 3	CASE 4
1	Cardiomegaly	0.82	0.06	0.09	0.11
2	Emphysema	0.70	0.47	0.04	0.93
3	Effusion	0.29	0.88	0.03	0.29
4	Hernia	0.83	0.56	0.06	0.16
5	Infiltration	0.34	0.55	0.28	0.42
6	Mass	0.26	0.75	0.06	0.80
7	Nodule	0.36	0.51	0.09	0.57
8	Atelectasis	0.18	0.32	0.06	0.49
9	Pneumothorax	0.19	0.85	0.06	0.91
10	Pleural Thickening	0.71	0.96	0.05	0.46
11	Pneumonia	0.19	0.46	0.09	0.23
12	Fibrosis	0.80	0.82	0.03	0.08
13	Edema	0.08	0.21	0.06	0.38
14	Consolidation	0.11	0.61	0.10	0.49

Emphysema is suggested with a substantial confidence score, hinting at lung air sac damage and potential chronic obstructive pulmonary disease. Hernia is confidently predicted, signaling organ protrusion through the abdominal wall, requiring clinical attention. Based on the predictions, there are indications that the patient may be at risk of certain cardiac and respiratory conditions.

For case 2, Cardiomegaly is predicted with a low probability, indicating a lower likelihood of an enlarged heart. Emphysema is suggested with a moderate probability, pointing to potential damage to air sacs and association with chronic lung conditions. Effusion shows a high probability, signifying a strong likelihood of fluid accumulation around the lungs, requiring immediate attention. Mass is predicted with a high probability, suggesting the presence of a tumor and necessitating immediate medical attention. Pneumothorax is predicted with a high probability, indicating a strong likelihood of air leakage into the pleural space, requiring urgent medical attention. Pleural Thickening is predicted with a very high probability, suggesting significant membrane thickening around the lungs and potential respiratory conditions. Fibrosis is predicted with a high probability, indicating scarring of

lung tissue and association with chronic lung diseases. Consolidation is moderately predicted, indicating a region of the lung filled with liquid, recommending further diagnostic tests and clinical evaluation.

For case 3, Infiltration is moderately predicted, suggesting substances in lung tissues, prompting clinical evaluation and additional tests. All other classes have a low probability prediction. Considering the low probability assigned to Cardiomegaly and the relatively lower probabilities of other cardiac-related conditions, the patient appears to have a lower overall risk of heart disease based on the model's prediction.

For case 4, Emphysema is predicted with a high probability, indicating a significant likelihood of lung air sac damage, prompting concerns about potential respiratory issues and necessitating further clinical evaluation. Mass is predicted with a high probability, indicating a significant likelihood of a tumor or abnormal growth, requiring urgent clinical correlation, imaging studies, and possibly a biopsy for accurate diagnosis and treatment planning. Nodule has a moderate to high probability, suggesting the possibility of small, rounded abnormalities in the lung, prompting the need for further diagnostic tests, such as CT scans.

Pneumothorax is predicted with a high probability, suggesting a significant likelihood of air leakage into the pleural space, necessitating urgent clinical evaluation and imaging studies for prompt intervention. Considering the collective probabilities and the relatively high probability of Emphysema, Mass, and Pneumothorax, there might be an increased risk of heart-related issues.

However, caution is required in cases where the model assigns lower probabilities, emphasizing the need for further investigation or potential model improvement. Additionally, the consideration of patient risk for heart disease, inferred from the results, adds a valuable layer of clinical relevance to the model's output.

6. Conclusion and Future Directions

The classification of chest diseases from CXR images have been conducted and presented in this research. The superior performance of the proposed deep CNN based on the DenseNet over the InceptionV3 and ResNet model structures have been demonstrated with several standard performance metrics including saliency feature maps and DenseNet based Grad-CAM with LIME visualizations. The classification and evaluation of the chest diseases from chest X-ray diagnostic image models for 14 different diseases using deep CNN based on DenseNet model structure have provided valuable insights into the potential applications of artificial intelligence in medical imaging. The model, trained on a diverse dataset, demonstrated varying probabilities for each detected condition. The findings indicate that the model has the potential to assist healthcare professionals in the preliminary assessment of chest X-rays, highlighting areas of concern and guiding further diagnostic efforts. Notably, the model identified elevated probabilities for different conditions such as Emphysema, Mass, Pneumothorax, and Atelectasis, suggesting a need for careful consideration and follow-up examinations.

It is crucial to emphasize that while the model predictions offer valuable information, they are not a substitute for direct professional medical diagnosis. The probabilities provided should be interpreted cautiously, and any conclusive medical decisions should be made by trained medical or healthcare practitioners. Moreover, the model's predictions may benefit from continuous refinement through ongoing training on diverse and representative datasets. As with any medical diagnostic tool, the ethical considerations of AI in healthcare must be acknowledged. Patient privacy, transparency, and the responsible deployment of AI technologies should be prioritized to ensure the ethical use of such systems.

As a future direction, enhancements could include refining the model architecture, incorporating additional data sources, and collaborating with healthcare professionals for real-world validation. As the field of medical AI advances, this work serves as a stepping stone towards the integration of intelligent diagnostic tools to augment the capabilities of healthcare providers. Ultimately, the success of this work lies in its potential to contribute to more efficient and accurate medical diagnostics. The journey of building and evaluating this model underscores the interdisciplinary collaboration needed between data scientists, healthcare professionals, and ethicists to harness the full potential of artificial intelligence in healthcare.

Careful selection of evaluation metrics aligned with clinical goals is vital. Sensitivity, specificity, and confusion matrices provide a nuanced understanding of the model's performance. Enhancing model interpretability through explainability techniques, like AD-CAM and Grad-CAM, enables visualization of regions of interest in X-rays [24].

Collaboration with healthcare experts, especially radiologists, pulmonologists, and cardiologists, is essential for nuanced interpretation and validation of results. Sharing knowledge and the code base with the research community, along with continuous learning from advancements in medical imaging and deep learning, ensures the longevity of research in this field.

Authors Contribution
All authors have contributed equally to prepare the paper.

Availability of data and materials
The data that support the findings of this study are available from the corresponding author, upon reasonable request.

Conflict of interests
The authors declare that they have no known competing financial interests or personal relationships that could have appeared to influence the work reported in this paper.

References

[1] Malik, H., Anees, T., Din, M., & Naeem, A., (2023). CDC_Net: multi-classification convolutional neural network model for detection of COVID-19, pneumothorax, pneumonia, lung

Cancer, and tuberculosis using chest X-rays, *Multimedia Tools and Applications*, 82, 13855 – 13880, Available: DOI: https://doi.org/10.1007/s11042-022-13843-7

[2] Olayiwola, J. O., Badejo, J. A., Okokpujie, K., & Awomoyi, M. E., (2023). Lung-Related Diseases Classification Using Deep Convolutional Neural Network, *Mathematical Modelling of Engineering Problems*, 10 (4), 1097 – 1104.

[3] Çall, E., Sogancioglu, E., Van Ginneken, B., Van Leeuwen, K. G., & Murphy, K., (2021). Deep learning for chest X-ray analysis: A survey, *In Medical Image Analysis*, 72, Elsevier B.V., London. Available: DOI: https://doi.org/10.1016/j.media.2021.102125

[4] Muhammad, T. N., Hussain, T., Lee, C. S., & Khan, M. A., (2022). Classification and Detection of COVID-19 and Other Chest-Related Diseases Using Transfer Learning, *Sensors*, 22 (7977), 1 – 18, Available: DOI: https://doi.org/10.3390/s22207977

[5] Ghosh, A., Sufian, A., Sultana, F., Chakrabarti, A., & De, D., (2020). Fundamental Concepts of Convolutional Neural Network, In: Balas, V., Kumar, R., Srivastava, R. (eds) Recent Trends and Advances in Artificial Intelligence and Internet of Things. *Intelligent Systems Reference Library*, 172, 516 – 567, *Springer*, Cham., Available: DOI: https://doi.org/10.1007/978-3-030-32644-9_36

[6] Krichen, M., (2023). Convolutional Neural Networks: A Survey, *Computers*, 12 (151), 1 – 41, Available: DOI: https://doi.org/10.3390/computers12080151

[7] Mienye, I. D., Swart, T. G., Obaido, G., Jordan, M. & Ilono, P., (2024). Deep Convolutional Neural Networks: A Comprehensive Review, Technical Report, Institute of Intelligent Systems, University of Johannesburg, *Johannesburg, Gauteng, South Africa*, 1 – 34, Available: DOI: https://doi.org/10.20944/preprints202408.1288.v1

[8] Khanam, R., Hussain, M., Hill, R., & Allen, P., (2016). A Comprehensive Review of Convolutional Neural Networks for Defect Detection in Industrial Applications, *IEEE Access*, 4, 1 – 47, Available: DOI: https://doi.org/10.1109/ACCESS.2024.3425166

[9] Miotto, R., Wang, F., Wang, S., Jiang, X., & Dudley, J. T., (2017). Deep learning for healthcare: Review, opportunities and challenges, *Briefings in Bioinformatics*, 19 (6), 1236 – 1246, Available: DOI: https://doi.org/10.1093/bib/bbx044

[10] Abbasi, S. F., Abbasi, Q. H., Saeed F., & Alghamdi, N. S., (2023). A convolutional neural network-based decision support system for neonatal quiet sleep detection, *Mathematical Biosciences and Engineering*, 20 (9), 17018 – 17036. DOI: https://doi.org/10.3934/mbe.2023759

[11] Beale, M. H., Hagan, M. T., & Demuth, H. B., (2025). Deep Learning Toolbox: User's Guide, *MATLAB & Simulink®*, 1 – 5258, 2025. *The MathWorks Inc*, *Natick*, *U.S.A.* www.mathworksa.com

[12] MathWorks. MATLAB & Simulink® 2025, The MathWorks Inc,Natick, U.S.A. www.mathworksa.com

[13] Pal, M., Parija, S., & Panda, G., (2024). An effective ensemble approach for classification of chest X-ray images having symptoms of COVID: A precautionary measure for the COVID-19 subvariants, *e-Prime – Advances in Electrical Engineering, Electronics and Energy*, 8 (100547), 1 – 17.

[14] Du, J., & Yang, J., (2023). Classification of Chest X-ray Images(Pneumonia) Based on ResNet and Grad-CAM, *SPML' 23: In Proceedings of the 6th International Conference on Signal Processing and Machine Learning*, 156 – 164, Avilable: DOI: https://doi.org/10.1145/3614008.3614031

[15] Karna, A., Jha, A., Dahal, A., Pandey, A., & Jha, T. N., (2023). Chest X-Ray Classification using DenseNet, In Proceedings of the 13th IOE Graduate Conference, Dharan, 13, 64 – 67.

[16] Kundu, R., Das, R., Geem, Z. W., Han, G. T., & Sarkar, R., (2021). Pneumonia detection in chest X-ray images using an ensemble of deep learning models, *PLOS ONE*, 16 (9), 1 – 29, Available: DOI: https://doi.org/10.1371/journal.pone.0256630

[17] Anushya, A., & Thai, P. L. T., (2024). Classification of Chest Disease Detection Using X-Ray Images through the Implantation of Efficientnetv2, *International Journal of Scientific Research in Engineering and Management*, 8, (11), 1 – 10.

[18] Nasser, A. A., & Akhloufi, M. A., (2022). Chest Diseases Classification Using CXR and Deep Ensemble Learning, *In CBMI'22: In Proceedings of the 19th International Conference on Content-based Multimedia Indexing, New York, U.S.A.* 116 – 120. Available: DOI: https://doi.org/10.1145/3549555.3549581

[19] Saha, O., Tasnim, J., Raihan, M. T., Mahmud, T., Ahmmed, I., & Anowarul, S. A., (2020). A Multi-Model Based Ensembling Approach to Detect COVID-19 from Chest X-Ray Images, *In 2020 IEEE Region 10 Conference (TENCON)*, Osaka, Japan. 591 – 595, Available: DOI: https://doi.org/10.1109/TENCON50793.2020.9293802

[20] Tang, Y. X., Tang, Y. B., Peng, Y., Yan, K., Bagheri, M., Redd, B. A., Brandon, C. J., Lu, Z. Han, M., Xiao, J., & Summer, R. M., (2020). Automated abnormality classification of chest radiographs using deep convolutional neural networks, *Digital Medicine*, 3 (70), 1 – 8. Available: DOI: https://doi.org/10.1038/s41746-020-0273-z

[21] Nasser, A. A., & Akhloufi, M. A., (2023). A Review of Recent Advances in Deep Learning Models for Chest Disease Detection Using Radiography, *Diagnosis*, 13 (159), 1 – 36, Available: DOI: https://doi.org/10.3390/diagnostics13010159

[22] Cardinale, L., Volpicelli, G., Lamorte, A., Martino, J., & Veltri, A., (2012). Revisiting signs, strengths and weaknesses of Standard Chest Radiography in patients of Acute Dyspnea in the Emergency Department, *Journal of Thoracic Disease*, 4 (4), 398 – 407, Available: DOI: https://doi.org/10.3978/j.issn.2072-1439.2012.05.05

[23] Long, R., Lau, A., Barrie, J., Winter, C., Armstrong, G., Egedahl, M. L., & Doroshenko, A., (2023). Limitations of Chest Radiography in Diagnosing Subclinical PulmonaryTuberculosis in Canada, *Mayo Clinic Proceedings: Innovations, Quality & Outcomes*, 7 (3), 165 – 170, Available: DOI: https://doi.org/10.1016/j.mayocpiqo.2023.03.003

[24] Iqbal, S., Qureshi, A. N., Alhussein, M., Aurangzeb, K., & Anwar, M. S., (2023). AD-CAM: Enhancing interpretability of conventional neural networks with a lightweight framework – From black box to glass box, *IEEE Journal of Biomedical and Health Informatics*, 28 (1), pp. 514 – 525.

[25] Mayats-Alpay, L., (2023). Artificial Intelligence for Automatic Detection and Classification Disease on the X-Ray Images, *Image and Video Processing (EESS.IV)*, 1 – 21, Available: http://arxiv.org/abs/2211.08244

[26] Pant, T. R., Aryal, R. K., Panthi, T., Maharjan, M., & Joshi, B., (*2021*). Disease Classification of Chest X-Ray using CNN, In *IEEE 6th International Conference on Computing, Communication and Automation (ICCCA), Arad, Romania*, 467 – 471, Available: DOI: https://doi.org/10.1109/ICCCA52192.2021.9666246

[27] Summer, R. M., NIH Clinical Center provides one of the largest publicly available chest x-ray datasets to scientific community, Images are available via

Box: https://nihcc.app.box.com/v/ChestXray-NIHCC. Retreived 15th January, 2025. Available: https://www.nih.gov/news-events/news-releases/nih-clinical-center-provides-one-largest-publicly-available-chest-x-ray-datasets-scientific-community.

[28] Wang, X., Peng, Y., Lu, L., Lu, Z., Bagheri, M., & Summers, M., (2017). ChestX-ray8: Hospital-scale Chest X-ray Database and Benchmarks on Weakly-Supervised Classification and Localization of Common Thorax Diseases, *IEEE CVPR*, 1 – 10. Available: https://openaccess.thecvf.com/content_cvpr_2017/papers/Wang_ChestX-ray8_Hospital-Scale_Chest_CVPR_2017_paper.pdf.

[29] Carter, P., Lagan, J., Fortune, C., Bhatt, D. L., Vestbo, J., Niven, R., Chaudhuri, N., Schelbert, E. B., Potluri, R., & Miller, C. A., (2019). Association of Cardiovascular Disease With Respiratory Disease, *Journal of the American College of Cardiology*, 73 (17), 2166 – 2177. Available: DOI: https://doi.org/10.1016/j.jacc.2018.11.063

[30] Osakwe, R. A. O., Akpan, V. A., & Babalola, M. T., (2017). Comparative Study of the Symptoms of Impending Human Heart, Kidney and Liver Failures Based on Blood Samples, *International Journal of Chinese Medicine (IJCM)*, 1(1), 32 – 44. Available: http://article.sciencepublishinggroup.com/pdf/10.11648.j.ijcm.20170102.11.pdf.

[31] Akpan, V. A., Omotehinwa, O. T., & Agbogun, J. B., (2022). Adaptive Classification of Impending Human Heart, Kidney and Liver Failures Based on Measurable Blood-Related Parameters Using MIMO HANFA-ART with ACA Algorithms, *Biomedical Sciences*, 8 (3), 97 – 112, Available: https://www.sciencepg.com/journal/paperinfo?journalid=362&doi=10.11648/j.bs.20220803.14.

[32] Kavitha, S. M., Thaarani, S., Singh, A. P., & Santhosh, G., (2023). Chest Disease Classification Using Convolutional Neural Networks, *In 2023 International Conference on Computer Communication and Informatics (ICCCI), Coimbatore, India.* 1 – 4. DOI: https://doi.org/10.1109/ICCCI56745.2023.10128179

[33] Hadhoud, Y., Mekhaznia, T., Bennour, A., Amroune, M., Kurdi, N. A., Aborujilah, A. H., & Al-Sarem, M., (2024). From Binary to Multi-Class Classification: A Two-Step Hybrid CNN-ViT Model for Chest Disease Classification Based on X-Ray Images, *Diagnostics*, 14 (23), 2754, 2024. Available: DOI: https://doi.org/10.3390/diagnostics14232754

[34] Koskela, R. S., Mutanen, P., Sorsa, J. A., & Klockars, M., (2005). Respiratory disease and cardiovascular morbidity, *Occupational and Environmental Medicine*, 62 (9), 650 – 655, DOI: https://doi.org/10.1136/oem.2004.017111

[35] AHA Electrocadiogram (ECG or EKG). American Heart Association, (2025). https://www.heart.org/en/health-topics/diagnosing-a-heart/electrocardiogram-ecg-or-ekg. Retrieved 12th February, Available [Online]: https://my.clevelandclinic.org/health/diagnostics/16953-electrocardiogram-ekg.

[36] Iqbal, S., Qureshi, A. N., Li, J., Choudhry, I. A., & Mahmood, T., (2023). Dynamic learning for imbalance data in learning chest X-ray and CT images, *Heliyon*, 9 (1), 1 – 20, Available: DOI: https://doi.org/10.1016/j.heliyon.2023.e16807

[37] Abiyev, R. H., & Ma'aitah, M. K. S., (2018). Deep convolutional neural networks for chest disease detection, *Journal of Healthcare Engineering*, 2018 (4168538), 1 – 11. DOI: https://doi.org/10.1155/2018/4168538

[38] Almezhghwi, K., Serte, S., & Al-Turjman, F., (2021). Convolutional neural networks for the classification of chest X-rays in the IoT era, *Multimedia Tools and Applications*, 2021 (80), 29051 – 29065. DOI: https://doi.org/10.1007/s11042-021-10907-y

[39] Lent-Schochet, D., & Jialal, I., (2023). Physiology, Edema, *Treasure Island (FL), StatPearls Publishing, Florida, U.S.A.* Available: https://www.ncbi.nlm.nih.gov/books/NBK537065/

[40] Saifullah, S., Yuwono, B., Rustamaji, H. C., Saputra, B., Dwiyanto, F. A. & Drezewski, R., (2023). Detection of Chest X-ray Abnormalities Using CNN Based on Hyperparameter Optimization, *In Proceedings of the 4th International Electronic Conference on Applied Sciences Session Computing and Artificial Intelligence, Italy*, 52, 1 – 8, Available: DOI: https://doi.org/10.3390/ASEC2023-16260

[41] Yen, C. T., & Tsao, C. Y., (2024). Lightweight convolutional neural network for chest X-ray images classification, Nature: Scientific Reports, Vol. 14, No. 29759, pp. 1 – 23, Available: DOI: https://doi.org/10.1038/s41598-024-80826-z

[42] Amin, H., & Siddiqui, W. J., (2023). Cardiomegaly, *Treasure Island, StatPearls Publishing, U.S.A.*, Available: https://www.ncbi.nlm.nih.gov/books/NBK542296/

[43] MacNee, W., (2006). Pathology, pathogenesis, and pathophysiology, *BMJ*, 332 (7551), 12024 .

[44] Karkhanis, V. S., & Joshi, J. M., (2012). Pleural effusion: diagnosis, treatment, and management, *Open Access Emergency Medicine*. 4, 31 – 52, Availble: DOI: https://doi.org/10.2147/OAEM.S29942

[45] Sabrina, F., (2025). *Understanding Hernias: the Basics*, Last updated (23rd ed.). December, 2022. Retrieved 17 February, 2025. Available: https://www.webmd.com/digestive-disorders/understanding-hernia-basics

[46] Miller, M. A., & Zachary, J. F., (2017). Mechanisms and Morphology of Cellular Injury, Adaptation, and Death, *Pathologic Basis of Veterinary Disease*, 2017, 2 – 43, Available: DOI: https://doi.org/10.1016/B978-0-323-35775-3.00001-1

[47] Kim, M. P., & Hofstetter, W. L., (2009). Tumors of the diaphragm, *Thoracic Surgery Clinics*, 19 (4), 521 – 529, Available: DOI:https://doi.org/10.1016/j.thorsurg.2009.08.007 https://www.researchgate.net/publication/41187480_Tumors_of_the_Diaphragm

[48] Gould, M. K., Donington, J., Lynch, W. R., Mazzone, P. J., Midthun, D. E., Naidich, D. P., & Wiener, R. S., (2013). *Evaluation of individuals with pulmonary nodules: when is it lung cancer? Diagnosis and management of lung cancer*, (3rd ed.). American College of Chest Physicians evidence-based clinical practice guidelines. Chest, 143(5), pp. e93S – e120S, 2013. DOI: https://doi.org/10.1378/chest.12-2351

[49] Grott, K., Chauhan, S., & Dunlap, J. D., (2023). Atelectasis, *Treasure Island, StatPearls Publishing, Florida, U.S.A.*, Available: https://www.ncbi.nlm.nih.gov/books/NBK545316/

[50] McKnight, C. L., & Burns, B., (2023). Pneumothorax, *Treasure Island (FL), StatPearls Publishing, Florida, U.S.A.*, https://www.ncbi.nlm.nih.gov/books/NBK441885/

[51] Pahal, P., Rajasurya, V., & Sharma, S., (2023). Typical Bacterial Pneumonia, *Treasure Island (FL), StatPearls Publishing, Florida, U.S.A.*, https://www.ncbi.nlm.nih.gov/books/NBK534295/

[52] T. A. Wynn and T. R. Ramalingam, "Mechanisms of fibrosis: therapeutic translation for fibrotic disease," Natural Medicine, Vol. 18, No. 7, pp. 1028 – 1040, 2012. Available: DOI: https://doi.org/10.1038/nm.2807

[53] Ahuja, J., Shroff, G. S., Mawlawi, Y., & Truong, M. T., (2019). Chronic Airspace Diseases, *Semin Ultrasound CTMR*, 40 (3), 175 – 186.

DOI: https://doi.org/10.1053/j.sult.2018.11.001

[54] Rehman, A., Khan, A., Fatima, G., Naz, S., & Razzak, I., (2023). Review on chest pathogies detection systems using deep learning techniques, *Artificial Intelligence Review*, 56 (11), 12607–12653, Available:
DOI: https://doi.org/10.1007/s10462-023-10457-9

[55] Jones, C. M., Buchlak, Q. D., Oakden-Rayner, L., Milne, M., Seah, J., Esmaili, N., & Hachey, B., (2021). Chest radiographs and machine learning – Past, present and future, *Journal of Medical Imaging and Radiation Oncology*, 65 (5), 538 – 544, Available:
DOI: https://doi.org/10.1111/1754-9485.13274

[56] Wang, Y. & Hargreaves, C. A., (2022). A Review Study of the Deep Learning Techniques used for the Classification of Chest Radiological Images for COVID-19 Diagnosis, https://www.sciencedirect.com/science/article/pii/S266709682200043X.

[57] Motamed, S., Rogalla, P., & Khalvati, F., (2021). Data augmentation using Generative Adversarial Networks (GANs) for GAN-based detection of Pneumonia and COVID-19 in chest X-ray images, *Informatics in Medicine Unlocked*, 27 (100779), 1 – 7, Available:
DOI: https://doi.org/10.1016/j.imu.2021.100779

[58] Kamrul, H., AshrafulAlam, M., Dahal, L., ToufickElahi, M. E., Roy, S., Redwan, W. S., Martí, R., & Khanal, B., (2022). Challenges of Deep Learning Methods for COVID-19 Detection Using Public Datasets, *Informatics in Medicine Unlocked*, 30 (100945), 1 – 11.
DOI: https://doi.org/10.1101/2020.11.07.20227504

[59] Meedeniya, D., Hashar, K., Shammi, K., Chamodi, F., Isabel, D., & Gonçalo, M., (2022). Chest X-ray analysis empowered with deep learning: A systematic review, *Applied Soft Computing*, 126 (109319), 1 – 20. https://pmc.ncbi.nlm.nih.gov/articles/PMC9393235/pdf/main.pdf

[60] Huang, G. H., Fu, Q. J., Gu, M. Z., Liu, K. Y., & Chen, T. B., (2022). Deep Transfer Learning for the Multilabel Classification of Chest X-ray Images, *Diagnosis*, 12 (1457), 1 – 18.
DOI: https://doi.org/10.3390/diagnostics12061457

[61] Sirazitdinov, I., Kholiavchenko, M., Kuleev, R., & Ibragimov, B., (2019). Data Augmentation for Chest Pathologies Classification, *In IEEE 16th International Symposium on Biomedical Imaging (ISBI) Venice, Italy*. 1216 – 1219.
DOI: https://doi.org/10.1109/ISBI.2019.8759573

[62] Ng, M. F., & Hargreaves, C. A., (2023). *Generative Adversarial Networks for the Synthesis of Chest X-ray Images, In 3rd International Electronic Conference on Applied Sciences*, 1 – 15 , 31, 84 – 90. Available: https://asec2022.sciforum.net/

[63] Keita, Z., (2025). What is a Convolutional Neural Network (CNN)? *Data Camp*, 1 – 6, Last updated 14th November, Retrieved on 15th February, 2025. Available [Online]: https://www.datacamp.com/tutorial/introduction-to-convolutional-neural-networks-cnns

[64] Tariq, F., (2023). Breaking Down the Mathematics Behind CNN Models: A Comprehensive Guide, *Medium*, 1 – 14. Last updated 2nd May, 2023. Retrieved on 15th February, 2025. Available [Online]: https://medium.com/@beingfarina/breaking-down-the-mathematics-behind-cnn-models-a-comprehensive-guide-1853aa6b011e

[65] Leo, C., (2025). The Math Behind Convolutional Neural Networks, *Medium*, TDS Archive, 1 – 43, Last update 9th April, 2024**.** Retrieved on 15th February, 2025**.** Available [Online]: https://medium.com/data-science/the-math-behind-convolutional-neural-networks-6aed775df076

[66] Huang, G. H., Liu, Z., Van, L., Maaten, D., & Weinberger, K. Q., (2017). Densely Connected Convolutional Networks, In *IEEE Conference on Computer Vision and Pattern Recognition (CVPR)*, Honolulu, HI, USA, 2261 – 2269.
DOI: https://doi.org/10.1109/CVPR.2017.243

[67] Ahmed, I., Jeon, G., & Chehri, A., (2023). An IoT-enabled smart health care system for screening of COVID-19 with multi layers features fusion and selection, *Computing (Special Issue Article)*, 105, 743 – 760.
DOI: https://doi.org/10.1007/s00607-021-00992-0

[68] Mujahid, M., Rustam, F., Álvarez, R., Mazón, J. L. V., Díez, I. D. L. T., & Ashraf, I., (2022). Pneumonia Classification from X-ray Images with Inception-V3 and Convolutional Neural Network, *Diagnostics*, 12 (1280), 1 – 16.
DOI: https://doi.org/10.3390/diagnostics12051280

[69] Kesuma, L. I., Ermatita & Erwin, (2023). ELREI: Ensemble Learning of ResNet, EfficientNet, and Inception-v3 for Lung Disease Classification based on Chest X-Ray Image, *International Journal of Intelligent Engineering and Systems*, 16 (5), 149 – 161.
DOI: https://doi.org/10.22266/ijies2023.1031.14

[70] Zak, M., & Krzyżak, A., (2020). Classification of Lung Disease Using Deep Learning Models, *ICCS, LNCS 12139*, 621 – 634.
DOI: https://doi.org/10.1007/978-3-030-50420-5_47

[71] Hossain, M. B., Iqbal, S. M. H. S., Islam, M. M., Akhtar, M. N., & Sarker, I. H., (2022). Transfer learning with fine-tuned deep CNN ResNet50 model for classifying COVID-19 from chest X-ray images, *Informatics in Medicine Unlocked*, 30 (100916).
DOI: https://doi.org/10.1016/j.imu.2022.100916

[72] Ahamed, M. K. U., Islam, M. M., Uddin, M. A., Akhter, A., Acharjee, U. K., Paul, B. K., & Moni, M. A., (2023). DTLCx: An Improved ResNet Architecture to Classify Normal and Conventional Pneumonia Cases from COVID-19 Instances with Grad-CAM-Based Superimposed Visualization Utilizing Chest X-ray Images, *Diagnostics*, 13(3), 1 – 28.
DOI: 10.3390/diagnostics13030551

[73] Onah, D. F. O., & Warsame, H. R. , (2024). Paediatric Pneumonia chest X-ray image classification with association to Lung cancer disease using ResNet50 Deep Learning Model, *In the Proceedings of the 2024 IEEE International Conference on Big Data (BigData)*, 15 – 18, Washington, DC, USA, 2024, 8859 – 8861.
DOI: https://doi.org/10.1109/BigData62323.2024.10825759

[74] Panati, C., Wagner, S., & Brüggenwirth, S., (2022). Feature Relevance Evaluation using Grad-CAM, LIME and SHAP for Deep Learning SAR Data Classification, *In the Proceedings of the 2022 23rd International Radar Symposium (IRS), Gdansk, Poland*, 457 – 462. Available [Online]:
DOI: https://doi.org/10.23919/IRS54158.2022.9904989

[75] Ennab, M., & Mcheick, H., (2025). "Advancing AI Interpretability in Medical Imaging: A Comparative Analysis of Pixel-Level Interpretability and Grad-CAM Models," *Machine Learning & Knowledge Extraction*, 7 (12), 1 – 32, DOI: https://doi.org/10.3390/make7010012

[76] Zhu, M., Zang, B., Ding, L., Lei, T., Feng, Z., & Fan, J. (2022). LIME-Based Data Selection Method for SAR Images Generation Using GAN, *Remote Sensing*, 14 (204), 1 – 14. DOI: https://doi.org/10.3390/rs14010204

[77] Raiaan, M. A. K., Sakib, S., Fahad, N. M., Mamun, A. A. Rahman, M. A., Shatabda, S., & Mukta, M. S. H., (2024). A Systematic Review of Hyperparameter Optimization Techniques in Convolutional Neural Networks, *Decision Analytics Journals*, 11 (100470).
DOI: https://doi.org/10.1016/j.dajour.2024.10047